Two Innovative Field Studies to Improve Transportation Safety: Vehicle-to-Infrastructure Reliability Testing and Analysis of Wind Forces on Cyclists

A Dissertation

Presented in Partial Fulfillment of the Requirements for the

Degree of Doctor of Philosophy

with a

Major in Civil Engineering

in the

College of Graduate Studies

University of Idaho

by

Fatma Elzahraa Madkour

Approved by:

Major Professor: Michael Lowry, Ph.D.

Committee Members: Ahmed Abdel-Rahim, Ph.D.; Kevin Chang, Ph.D.

Vibhav Durgesh, Ph.D.

Department Administrator: Fritz Fiedler, Ph.D.

December 2021

Abstract

Each year vehicle collisions are the second leading cause of unintentional death worldwide (following poisoning as the first leading cause). In 2019, 36,096 people died in the United States due to vehicle collisions, including 6,205 pedestrians and 846 cyclists. The same year, there were 66,000 injuries from vehicle collisions. The US Department of Transportation dedicates significant annual financial investment to provide safer streets and improve driving behavior to reduce crashes and fatalities. This dissertation presents two studies aimed at improving transportation safety and reducing crashes. Both studies involved field observations and laboratory simulation. The first study focused on developing a new method for safety reliability testing for connected vehicles-to-infrastructure. The main goal of this study was to enhance V2I communications to decrease vehicle rashes at signalized intersections. The second study investigated safety issues for cyclists when vehicles pass them and exert wind forces to eliminate cyclist-vehicle crashes in rural areas.

The first study created an innovative method to test the reliability of vehicle-to-infrastructure (V2I) communications in connected vehicles at traffic signals. The new method provides an alternative to using the communication data reported by proprietary vendor-supplied interfaces. This vendor independent method is based on a rigorously tested translation model that uses measured Received Signal Strength Indicator (RSSI) from any V2I communication equipment to predict the corresponding Packet Delivery Ratio (PDR). This was achieved by correlating the signal strength, measured using a generic power meter, to PDR values reported in the communication interface of the equipment of different vendors. Both stationary and in-motion (10 to 40 mph) field data collection tests were conducted at three traffic intersections. These tests were performed over distances of up to 500 meters between the Roadside Units (RSUs) and the On-Board Units (OBUs). The results were statistically analyzed and logistic and linear regression models that predict PDR values were developed. A case study in the field to test and validate this new PDR prediction model was conducted at two intersections in Boise, Idaho. Our prediction model will enable transportation system operators to test and validate the efficiency of connected vehicle RSU/OBU communications at signalized intersection approaches under different traffic conditions, independent of vendor-provided tools.

The second study of this research is related to the understanding of the unsteady wind flow exerted on cyclist by passing vehicles. The impact to cyclists from the wind generated by passing trucks has not been investigated before in the USA. In 2018, there was 846 bicyclists killed in crashes with motor vehicles in the USA with an increase of 32% of pedestrian and cyclist fatalities between 2008 and

2018. The aerodynamic loads generated from moving vehicles trigger a concern on the stability and safety of cyclists which might lead to loss of control and consequently cyclist injury. The results of this study will help identify factors to mitigate safety concerns in rural and urban areas. The key parameters investigated were the relative speed between cyclist and truck (25, 40, and 60 mph), vehicle type (semitrailer, Single unit truck, SUV, and pick-up truck), separation distance spacing between cyclist and the truck (2 ft., 4 ft, and 6 ft.), and various cyclist types. The difference between the single unit truck and the semitrailer are the gross weight, the frontal area and the overall dimensions. The transverse wind and longitudinal wind speeds have been used to drive equivalent transverse and longitudinal forces using the aerodynamic principles and therefore the flipping moment experienced by a cyclist. The data was generated through intensive field tests in controlled and uncontrolled environments. In addition, computational fluid dynamics models were built to investigate computer simulations in predicting forces on cyclists. Finally, a physical three-dimensional model of a scaled truck and cyclist were created and tested in a wind tunnel under the same environments that have been used in the computer simulations. The modeling is based on wind speed equations that are a function of vehicle speed, separation distances, and vehicle type. The equations were derived based on the data collected from the field and was validated using the uncontrolled data set. In addition, flipping moment charts have been developed for each type of the vehicles to offer a strong evidence of quantified flipping moments experienced by cyclists under various conditions. The computer simulations concluded that it is feasible to use computational fluid dynamics to model the whole environment of various wind speeds and separation distances for typical cyclists. Strong correlation between the computer simulations and the wind tunnel tests have been obtained. Regardless of the scale effect, the overall results from the field tests and the computer simulations and the wind tunnel are showing the same trend in terms of transverse and longitudinal wind forces experienced by cyclists.

Acknowledgements

I would like to express my deep thanks and sincere appreciation to Dr. Michael Lowry for being my mentor throughout the planning and enhancement of this thesis. Dr. Lowry was eager to provide support and encouragement with patience for me during my research period. Without his endless guidance, and constructive advice this work would not have been accomplished.

I would also like to extend my thanks to the respectable committee members, Dr. Ahmed Abdel-Rahim, Dr. Kevin Chang, and Dr. Vibhav Durgesh for being part of my esteemed committee and for providing me with their valuable comments and feedback for improving my work's quality. I would like to deeply thank Ahmed Hammad and Pauolo Yu who greatly helped in the CFD analysis and during the wind tunnel testing.

I lovingly would like to extend my gratitude to my parents. Without their love, dedication, endless support, and prayers, it would have been impossible to achieve so much in my life. Last but not least, truly unbounded thanks are due to my generous husband for his continuous support, encouragement, and being patient in difficult times. I would also like to sincerely apologize to my son because for being busy at work all the time, and I hope he appreciate it one day that this was for the good of us all.

Dedication

This dissertation is dedicated to my beloved parents, and my beloved kids, they were

and will always be my greatest support in life.

Table of Contents

List of Tables

List of Figures

Chapter 1: Introduction

1.1 Enhancing Transportation Safety

The World Health Organization (WHO) reports [1] that 1.35 million people die each year because of road traffic crashes and that vehicle collisions are the second leading cause of unintentional death worldwide (following poisoning as the first leading cause of unintentional death). The 2030 WHO goal is to decrease the number of crashes by 50%. The cost of traffic crashes is reported to be 3% of Gross Domestic Product. In the USA, 36,096 deaths were reported in 2019 with 11.0 deaths per 100,000 population. In the state of Idaho, 73% of the 188 fatal vehicle crashes occurred in Idaho rural areas as reported by Insurance Institute for Highway Safety (IIHS) [2].

The National Highway Traffic Safety Administration (NHTSA) [3] reported that the economical and societal cost of traffic crashes is $871 B in a single year. Therefore, transportation safety and saving lives of people is a major topic that needs to be studied and enhanced further.

This dissertation presents two research studies to enhance transportation safety. Both studies include significant field observations and laboratory simulations. The first study is about vehicle-to-infrastructure (V2I) communications at traffic signals. The results from the study can help improve safety by providing a means for V2I reliability testing at signalized intersections. The second study is about the adverse wind flow exerted on cyclist by passing vehicles. The results provide important understanding to guide the development of crash mitigation strategies for cyclists in rural and urban areas.

1.2 Vehicle-to-Infrastructure Study Objectives

Equipping vehicles with communication capabilities has been in progress for more than four decades. Connected vehicle research started in the 1980s with basic communications of in-vehicle phones to cell towers and evolved to a full range of vehicle-to-vehicle and vehicle-to-infrastructure data exchange using dedicated short-range communications (DSRC). The wireless devices that implement DSRC technology in a connected vehicle (CV) environment are referred to as on-board units (OBUs) and road-side units (RSUs). The former are devices installed in vehicles to enable their inter-communication, as well as their communication to infrastructures through RSUs that are usually mounted on traffic light poles to provide communications with the vehicles' OBUs.

The main objectives of this study were focused on the evaluation and the reliability of RSU/OBU communications using results from field tests at signalized and non-signalized intersections located at

different terrains/environments with different speed limits. Contour maps were developed to visualize the Received Signal Strength Indicator (RSSI) and Packet Delivery Ratio (PDR) values from the collected field data. The developed models correlated the measured RSSI values using a generic power meter, with the RSSI and PDR values obtained from the vendors' communication interfaces. In addition, a proposed generalized equation was developed to directly predict the PDR given the RSSI sensed by the power meter for any vendor. Finally, the developed model was verified in the field based on a case study conducted in Boise, Idaho using CV equipment from two vendors. The study provided recommendations on how to re-use the models and methods developed in this study for vendor-independent performance evaluation of CV equipment.

1.3 Wind Force Study Objectives

The Wind Force Study presents an analysis of wind pressures that are exerted on cyclists due to passing vehicles. The tasks of this research were to measure the longitudinal and transverse wind speeds on a cyclist. The wind speeds generated from various vehicle types and separation distances at various vehicle speeds were used to develop corresponding forces and titling moments on cyclists and provide recommendations for cyclists' safety.

Safety of cyclists is one of the major concerns that attract the attention of department of transportation and stakeholders. In 2019, 846 cyclists have died due to the involvement in vehicle accidents (NHTSA) [3]. In addition, the medical expenses of fatal and non-fatal cyclist crashes were $237B over 17 years period (NHTSA). In the USA, the safety of cyclists in rural areas who overtaken by vehicles is not fully investigated.

The main objective of this study was to perform field tests and computer simulations to investigate the unsteady wind forces and flipping moments generated by passing various vehicle types at various speeds and separation distances between the cyclist and the vehicles. The field tests were conducted using an ultrasonic wind sensor that was mounted at a height corresponding to the center of gravity of a cyclist. The results of the study were used to develop wind force prediction equations and flipping moment charts for future recommendations and countermeasures of cyclist safety on roadways. In addition, the computer simulations have proven that it is feasible to model such a problem and wind forces could be generated and quantified.

1.4 Research Contribution Originality and Significance

The overall objective of this work was to provide solutions and countermeasures to improve transportation safety.

The main contribution of the V2I study is the creation of new testing models for reliability. The models correlate the RSSI values, measured using a generic power meter, with the RSSI and PDR values obtained from the vendors' communication interfaces. This work is significant because of the lack of commercial tools that can directly measure the PDR of RSU's/OBU's other than the vendors' own communication interfaces. The new approach will provide generic data stream (and thus vendor-independent) scheme to assess the reliability of V2I communications.

The following points summarize the contributions of this study:

- Evaluated the reliability of RSU/OBU communications using results from field tests at signalized and non-signalized intersections located at different terrains/environments with different speed limits.
- Visualized the RSSI and PDR values from the collected field data using contour maps.
- Developed models to correlate the RSSI values, measured using a generic power meter, with the RSSI and PDR values obtained from the vendors' communication interfaces.
- Proposed a generalized equation by combining the correlation models that can directly predict the PDR given the RSSI sensed by the power meter for any vendor.
- Validated and tested the developed model using field data collected at two signalized intersections in Boise, Idaho, using CV equipment from two vendors.
- Provided recommendations on how to re-use the models and methods developed in this study for vendor-independent performance evaluation of CV equipment.

The main contribution of the wind force study is field and simulated measurements of wind forces that impact cyclist stability. The highway safety manual does not provide information related to this topic and the results will provide data to cover this gap.

The specific contributions of this study are:

- Original research study that included various parameters (semitrailer truck, single unit truck, SUV, and pickup truck) to investigate wind forces and flipping moments on typical cyclists.
- Quantify wind force levels generated by moving vehicles through real field tests, scaled computer simulations, and using 3D printing technology in wind tunnel experiments.
- Determine how changes of vehicle speed, separation distance, vehicle types and various cyclist projected side areas affect the wind and force levels on a cyclist.
- Suggest solutions that might be implementable for cyclist safety.

1.5 Dissertation Outline

The next two chapters present each study as independent and self-contained descriptions. The chapters include background information, explanation of the methods, description of the results, conclusions, and discussion of future work. Chapter 2 is a modified version of a paper that was published in *Transportation Research Record*:Journal of the Transportation Research Board. Chapter 3 is a modified version of a manuscript that has been submitted for publication in a transportation journal. Chapter 4 provides conclusions and final comments for this dissertation as a whole.

Chapter 2: Reliability Testing Vehicle-to-Infrastructure Communications

Madkour, Fatma Elzahraa, Umair Mohammad, Sameh Sorour, Mohamed Hefeida, and Ahmed Abdel-Rahim. "Vendor-Independent Reliability Testing Model for Vehicle-to-Infrastructure Communications." Transportation Research Record 2674, no. 9 (September 2020): 898–912. https://doi.org/10.1177/0361198120932910.

2.1 Introduction

Equipping vehicles with communication capabilities has been in progress for more than four decades. It started in the 1980's with basic communications of in-vehicle phones to cell towers and evolved to a full range of vehicle-to-vehicle (V2V) and vehicle-to-infrastructure (V2I) data exchange using dedicated short-range communications (DSRC). The wireless devices that implement DSRC technology in a connected vehicle (CV) environment are referred to as on-board units (OBUs) and road-side units (RSUs). The former are devices installed in vehicles to enable their inter-communication, as well as their communication to infrastructures through RSUs that are usually mounted on traffic light poles to provide LOS communications with the vehicles' OBUs.

Initiatives to deploy CV technologies in cities have increasingly been considered by different transportation departments, including the United States Department of Transportation (USDOT) and a large number of states' DOTs [1]. The USDOT, for example, recently supported three preliminary CV test locations in New York, Wyoming, and Florida to evaluate the effectiveness of CV applications [1]. A CV safety pilot platform has also been started in Ann Arbor, Michigan in 2012 [2-5]. The Wyoming DOT program has included DSRC-OBU connectivity as part of a CV freight corridor implementation [6]. Tampa-Hillsborough Expressway Authority in the state of Florida has deployed V2V and V2I applications to reduce collisions and wrong-way entry using DSRC as the data communication medium [7]. These initiatives aim to provide DOTs with all operational, performance, and reliability studies to help accelerate the deployment of V2I technologies especially at intersections where most accidents occur. Among these diverse initiatives to test CV technologies are urgent calls from US DOT [8] and a collation of state DOTs [9] to test the reliability of wireless devices (i.e., RSUs and OBUs) developed by different vendors. In addition to the OBU/OSU units, CV traffic signal systems have various other crucial components including: Signal Phase and Timing (SPAT), Geometric Intersection Description (GID) data broadcast, Vehicle Awareness Devices (VADs), Aftermarket Safety Devices (ASDs), and the USDOT preliminary Security Credentials Management System (SCMS) [9].

Two main key performance indicators are usually considered to assess the quality and reliability of V2I communications (i.e., between OBUs and the RSU): Received Signal Strength Indicator (RSSI) and Packet Delivery Ratio (PDR). The RSSI assesses the level of power with which the signal is

received on either device, which highly correlates the ability of the receiver to detect the content of the signal with minimal to no errors. Conversely, PDR is the ratio of the number of successfully received packets to total number of packets sent. Reliability tests for V2V and V2I communications are typically performed as a function of distance between the two communicating devices in either LOS or non-LOS (NLOS) scenarios. Measuring RSU/OBU communication quality indicators (e.g., PDR) requires detection of specific fields in the data streams exchanged between the RSU and the OBU. Unfortunately, despite efforts to standardize, vendors set these fields in different proprietary ways. As a result, locating and accessing this specific data is quite complicated and time consuming, particularly for DOTs and municipalities' employees who are not typically experts in communication protocols and data structures.

Ching et al. [10] characterized RSU transmission power inside a tunnel for different lanes at different distances from RSU's placed at heights of 6.2 m and 8.0 m. The OBU was placed on a van at a height of 2.5 m. The characterization was performed by drawing power maps for each lane and scatter analysis was performed to understand the different contributions of power to each lane at different RSU heights. Daniel et al. [11] showed that the OBU successfully displayed a speed limit cross alert by generating a warning if speed exceeds the limit in a specific geographical area.

Zheng et al. [12] performed a simulation-based study of PDR and delay (packet transmission time) versus vehicle speed for different numbers of vehicles in highway environments. The results showed that for up to 2 vehicles at a time, speed did not have a significant impact on delay and PDR. Teixeira et al. [13] developed a simulated experimental analysis of DSRC with external antennas transmitting in the DSRC range mounted on two vehicles. One vehicle was kept stationary while the other was moving at different speeds. This is similar to [14], where the authors evaluated the impact of spectrum sharing. They placed a Wi-Fi device next to their DSRC device and evaluated the corresponding PDR. They also tested mitigation/sharing algorithms and reported the PDRs for different volumes of Wi-Fi traffic. The work in [15] evaluated the performance of Linkbird devices operating in the frequency band of 5.725-5.925 GHz in both highways and suburban streets in Pisa and Florence, Italy. The work in [16] is the most relevant to the scope of this study, where the authors characterized the RSSI and PDR versus the transmitted power. However, this was performed for a maximum transmission power of 33dBm. The characterization was done for urban and suburban environments in San Jose and Sunnyvale, CA, at different OBU-RSU distances.

In this study, we introduce a new model that uses measured RSSI values to predict the correspondent PDR values and hence assess the reliability of the communication between any two CV devices. Our model will enable transportation system operators to test and validate the efficiency of RSU/OBU

communications at signalized intersection approached under different traffic conditions without the need to use proprietary vendor-provided tools.

2.2 Methods

This study aims at developing a vendor-independent approach to test and validate the reliability of the communication between different CV devices in traffic signal system applications without enduring the complications of unraveling the individual technicalities of each vendor or basing the evaluation on values reported by the vendor's own communication interfaces. Indeed, measuring most quality indicators (e.g., packet delivery ratio - PDR) typically requires detection of specific fields into data streams exchanged between the RSU and the OBU. Unfortunately, different vendors set these fields in different ways despite of the standardization efforts. Locating and accessing this specific data is quite complicated and time consuming, particularly for DOTs and municipalities' employees who are not typically experts in communication protocols and data structures. This is also one of the reasons why, to the best of the authors' knowledge, no tools are currently available in the market that can directly measure the PDR of RSU's/OBU's other than the vendors' own communication interfaces.

The proposed approach will thus alleviate these technical burdens by providing a generic data stream (and thus vendor-independent) scheme to assess the reliability of V2I communications. To the best of our knowledge, this is the first attempt to characterize the relationship between RSSI and PDR independent of transmitted power, and most importantly, independent of vendor-specific interfaces and tools. To this end, this study develops a vendor-independent reliability testing approach for LOS V2I communication devices developed by different vendors and approved for testing and possible operation (upon passing the testing requirements) in the United States.

To achieve this goal, both stationary and in-motion (10 to 40 mph) field data collection tests were conducted using both vendor tools and a vendor-independent power meter. These tests were implemented in actual traffic intersections where the RSU was mounted on a traffic pole (or at a comparable height and location), and the OBU was placed inside a vehicle with the wireless antenna placed on top of the vehicle. For one of the vendors, both the RSSI and PDR were measured as a function of the LOS distance of the OBU from the RSU, using a dedicated vendor tool. Simultaneously, the RSSI at the OBU was collected using a generic power meter.

All test results, their interpretations in terms of reliability, and their comparison across the employed vendor devices were provided in the study for both dissemination and potential use by the different DOTs to assess their capability and quality of service (QoS). Moreover, regression techniques were employed on the collected data to develop a generalized prediction equation of the PDR as a function

of the RSSI input from a generic power meter. The new model we derived provides PDR predictions with a root-mean-square error (RMSE) of 2.21% and R^2 of 0.89. This model can thus be widely employed by DOT and municipalities to accurately compare the performance of different vendors' equipment in their own environments, without dealing with the individual technical complications of each vendors' devices and data streams.

The following points summarize the main contributions of this study:

- Evaluated the reliability of RSU/OBU communications using results from field tests at signalized and non-signalized intersections located at different terrains/environments with different speed limits.
- Visualized the RSSI and PDR values from the collected field data using contour maps.
- Developed models to correlate the RSSI values, measured using a generic power meter, with the RSSI and PDR values obtained from the vendors' communication interfaces.
- Proposed a generalized equation by combining the correlation models that can directly predict the PDR given the RSSI sensed by the power meter for any vendor.
- Validated and tested the developed model using field data collected at two signalized intersections in Boise, Idaho, using CV equipment from two vendors.
- Provided recommendations on how to re-use the models and methods developed in this study for vendor-independent performance evaluation of CV equipment.

2.3 Data Collection

The data collection from field observations was performed in two stages. The first stage was conducted using a vendor tool. Both the RSSI and PDR were measured as a function of the line-of-sight (LOS) and non-line-of-sight (NLOS) distance between the OBU and RSU, where the OBU was kept stationary (static test) and at various speed limits (mobile test). (The NLOS situations occurred due to an obstacle in the RSU-OBU path such as a tree.) The second stage of the data collection was conducted by measuring the RSSI from the RSU using a specific vendor's tool and a generic power meter under the same field conditions of the first stage tests (same distances, same traffic volumes, intersection types, etc.).

2.3.1   Stationary Data Collection

As described above, the goal of these tests was to relate the PDR to the RSSI measured by an independent RF power meter. Typically, it is expected that the relationship between the PDR and the RSSI should be consistent. However, it is possible that the RSSI may be different at the same distance from an RSU at two different intersections even when the cars (OBU's) are stationary or travelling at

the same speed. This is due to communication channel parameter variations with different types of obstacles (i.e., trees, buildings, light poles, etc.). Furthermore, in case of roads with different speed limits, the OBU's speed as well as the speed of objects around it affect the channel parameters controlled by the rate of fast fading due to the doppler effect. In light of these observations, we decided to perform the tests on at least the three types of intersections that can commonly be found in various parts of the world: commercial, suburban and rural. Therefore, it was crucial to evaluate the RSSI at each type of intersection and hence, one of each type was chosen for demonstration purposes.

The tests were done at three different types of intersections located in the city of Moscow, Idaho. The first intersection was a signal-free all-way stop at a residential/suburban 4-leg intersection (6th and Blaine Streets). Each intersection leg had two lanes of width 24.00 ft. (7.30 m), and a maximum speed limit of 25 mph (40.2 kph). The second location was a signalized commercial 4-leg intersection (Blaine Street and Troy Road-Hwy 8). The intersection is a 4- lanes and has a speed limit of 35 mph (56.3 kph). The third location was a rural 3-leg intersection (Mountain View Road and Darby Road) with a speed limit of 45 mph (72.2 kph). The terrain for the last intersection was a mixture of flat land and rolling hills without any obstacles (no trees or buildings). All intersections are shown in Figures 2.1 (a)-(c).

At every intersection, the RSU was mounted on a 12 ft. (3.66 m) high tripod as shown in Figures 2.1 (d)-(f). This height is comparable to that of a standard traffic signal. The OBU was placed inside the vehicle while its antenna was mounted on the vehicle's roof as shown in Figure 2.1g and Figure 2.1h. At the residential and commercial intersections, we divided every leg into 50 points (49 segments) that were 5.00 m (16.40 ft.) apart. On the other hand, the rural intersection was divided into 32.80 ft. (10 m) intervals up to 1640.42 ft. (500.00 m) away from the RSU. The reason for the larger distance span in the third intersection was to provide reliable communications for much longer distances.

Figure 2.1 Aerial view of all intersections.
RSU placement at each intersection and illustration of OBU antenna placement on the car. (a) Aerial view of the residential intersection. (b) Aerial view of the commercial intersection. (c) Aerial view of the rural intersection. (d) RSU position at the residential intersection. (e) RSU position at the commercial intersection. (f) RSU position at the rural intersection. (g) Front view of the OBU antenna on top of the vehicle. (h) Side view of the OBU antenna on top of the vehicle.

2.3.2 Mobile Data Collection

In this field test, the data was collected only at the third (rural) intersection at Mountain View Road with Darby Road, Moscow, Idaho. The set up and distance (i.e., half a mile away from the RSU at each intersection leg) for this data collection session was similar to that of the stationary test, except that the vehicle with the OBU was travelling at various speeds of 10, 20, 30, and 40 mph, which

represent typical operating speeds in urban corridors. At each speed, thirty round trips were carried out for each leg.

2.3.3   Power Meter Test

This data collection test involved the measurements of the RSSI at different distances from the RSU using both the vendor's tool (through the OBU) and the power meter. The test was conducted at the University of Idaho campus in two steps: 1) readings were collected through the OBU every 5 m (16.40 ft.), where every reading was taken by making a complete stop, and 2) readings were taken again (at the same locations of the first step) using the generic power meter. The OBU was turned off during the power meter data collection to avoid interference and thus inaccurate power readings. The two steps were conducted under identical conditions.

2.4 Results and Discussions

2.4.1   Stationary Test Results

The data collected from the static test is introduced in this section along with the corresponding analysis. The available vendor tool showed the received packet numbers in a sequence. Therefore, the lost packets could be calculated as shown by the procedure highlighted in Equations (2.1)-(2.3).

$$S = x_N - x_1 + 1 \tag{2.1}$$

Consider the set of packet sequence numbers $\{x_1, \ldots, x_i, \ldots, x_N\}$ where x_i is the sequence number of the jth sent packet for $i = 1, \ldots, N$. Then, the total number of sent packets from the RSU S can be calculated using Equation (2.1), where x_N represents the sequence number of the last packet sent and x_1 the first, respectively. On the other hand, the number of packets received by the OBU was calculated by counting the number of sequences as shown in Equation (2.2), where a total of R sequences is received by the OBU.

$$R = \left| \{x_1, x_2, \ldots, x_j, \ldots, x_R\} \right| \tag{2.2}$$

The element x_j represents the sequence number of the jth packet for $j = 1, \ldots, R$, and these sequence numbers form the set of received packets. The number of packets dropped, D, is given by Equation (2.3), which is simply the difference between the sent and received packets, S and R, respectively.

$$D = S - R \tag{2.3}$$

The PDR was calculated by dividing the number of successfully received packets by the number of sent packets as shown in Equation (2.4). The average RSSI of packets (denoted by RSSI) received at any given distance was calculated using Equation (2.5).

$$\text{PDR} = \frac{R}{S} \tag{2.4}$$

$$\text{RSSI} = \frac{\sum_{j=1}^{R} \text{RSSI}_j - (-110 * D)}{R} \text{ [dBm]} \tag{2.5}$$

Since the vendor tool could not report the RSSI of dropped packets, it was assumed dropped packets had a power of -110 dBm (minimum power recorded by the power meter at which a packet was successfully received). Consider the set of received RSSI measurements corresponding to the set of successfully decoded packets {RSSI1, …, RSSIj, …, RSSIR}. The second term of the numerator in Equation (2.5) eliminates the received power (which is -110 dBm) during the event of dropped packets. This calculation is vital for accurate measurements of RSSI at low received powers (below -110dBm).

At each point (station) of the considered intersection, two PDR and RSSI values were calculated based on Equations (2.1) to (2.5). When building the regression models, 80% of these calculated PDR and RSSI values (359 data points) were considered for training, whereas the remaining 20% of the data points (89 data points) were employed for validating the accuracy of the derived models. Two groups of data points were defined as the training and testing data points, respectively. A growth logistic model was developed to fit the training data by calculating the parameters in the logistic growth formula as shown in Equation (2.6).

$$\text{E(PDR)} = \frac{Q}{1 + e^{-\alpha(\text{RSSI}-\beta)}} \tag{2.6}$$

The following list describes the variables and the quantities they represent:
- *E(PDR):* Expected output of the logistic model for data fitting (dependent variable)
- *Q*: The value of the PDR as the RSSI approaches infinity (independent parameter)
- α: RSSI decay constant, (independent parameter)
- β: RSSI of the symmetric inflection point (independent parameter)

The derived regression parameters were $Q = 0.99$, $\alpha = 0.48$, and $\beta = -104.46$, which achieved an RMSE of 6.0 % and R^2 value of 0.96. Figure 2.2a shows the actual data (stationary test) with

training and testing points, while Figure 2.2b shows the trained data fitted to the regression model. The test data points were then used to ensure the validity of the developed model with the aforementioned values of Q, α and β as shown in Figure 2.2c. The model was able to predict the PDR with an RMSE of 7.7% and the R^2 was found to be 0.95.

The logistic model curve in Figure 2.2c could be divided into three different zones, namely a linear zone on the left (below -104 dBm), a transition zone in the middle (between -104 and -97 dBm), and a saturation zone (larger than -97 dBm). Calculating the RMSE across the three zones showed that the RMSE of the saturation zone was the lowest (4%), whereas the highest was attributed to the transition zone (18%), and the linear zone RMSE was 8.25% as shown in Table 2.1.
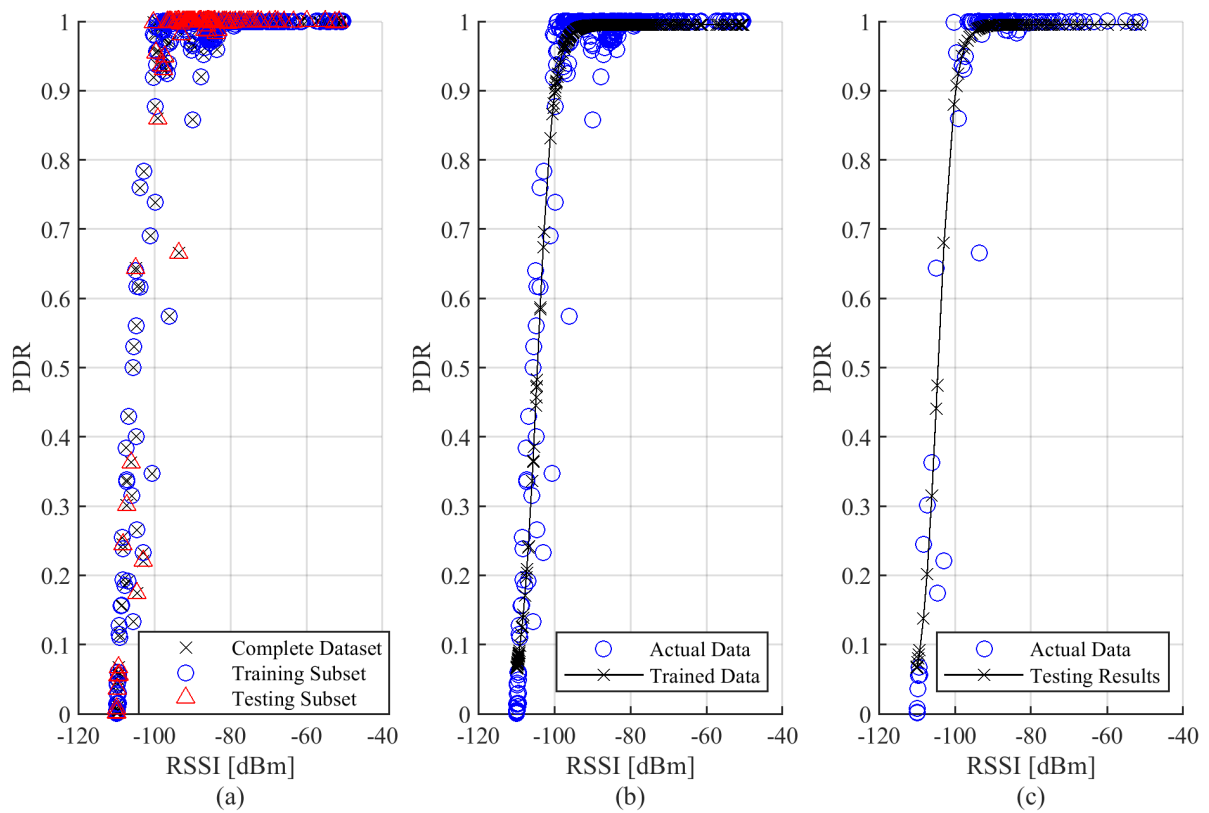
Figure 2.2 Illustration of the training and testing data
Split of the complete dataset for PDR versus RSSI and subsequent fitting/testing results using a logistic model (a) The complete dataset with train/test split (b) Logistic Model fitted/trained data (c) Tested data with the calibrated regression model.

Table 2.1 Statistical summary of the logistic zones for the stationary test

	Stationary Test Result		
	Linear	**Transition**	**Saturation**
	Region	Region	Region
RMSE (%)	8.25	18.00	4.00
R^2	0.95	0.88	0.99
	Total		
RMSE	7.7%		
R^2	0.95		

Table 2.2 shows the PDR variations associated with each of the aforementioned zones. Within the saturation zone, the PDR was in the range of 98.99% to 100%. As the RSSI approaches the transition zone, the PDR dropped from 98.99% to 38%, and continued to drop from 38% to 0.0% in the linear zone.

Table 2.2 RSSI range vs. PDR for the stationary test

Stationary	
RSSI (dBm)	**PDR**
-51.4→ -96	100%→ 98.99
-97→ -104.46	98.99%→ 38%
-104.46→ -110	38%→ 0%

The lowest error occurred in the saturation region which was very important as it showed that once the received power (in dBm) was beyond a certain threshold, a nearly perfect PDR could be achieved. Similarly, the mean square error was less than 10% in the low power region. Furthermore, by inspection, it was observed that the data points did not deviate from the general trend of the model used to fit the data. Therefore, we could say with confidence that logistic fitting was a good method for modeling the relationship between PDR and RSSI at very high and low power levels. In the middle ranges, between -105 to -95 dBm, the error was higher with visible outliers. There were several reasons for this as highlighted below.

One of the main reasons was because the transition zone was very small compared to the linear and saturation regions. Therefore, the model might not be able to capture such sharp change accurately. Furthermore, since the PDR could perform so well or degrade rapidly on either side of this

zone, in some cases the packet might be decoded correctly at even lower power levels and vice versa. Moreover, small errors in measurement might also appear as significant outliers. More data points were needed to accurately predict the behavior in the transition zone. Although the RMSE was high, the individual error in PDR measurements were very low (within 0.1%). Because of this and the simplicity of this approach compared to, for example, piece-wise modeling with polynomial fitting for the transition zone, logistic fitting is more feasible. Lastly, below a certain PDR threshold, the communication could be rated unreliable, hence, an exact value might not be needed in the transition zone.

2.4.2   Contour Maps

Colored contour maps of RSSI and PDR were generated for the three different intersections (residential, commercial, and rural area) that have been considered in this study. These maps helped visualize the data collected to determine signal strength at different distances from the intersection and the received power threshold at the OBU.

Figures 2.3a and 2.3b show the RSSI and PDR contour maps, respectively, for the residential area (Blaine Street and 6th Street intersection). For the west leg of the intersection, the power decreased from -60 to -80 dBm when the distance was increased to 110 meters from 5 meters. The strength of the signal dropped significantly when the OBU was moved 135 meters away from the RSU, and it increased back between 140 to 190 meters to within the range -92.3 to -85 dBm, respectively. Finally, it dropped down again at 250 meters to -107.3 dBm. This unusual up and down fluctuation in the signal strength along the intersection's west leg was due to the intensive number of trees found along the sidewalk. In spots where trees were not blocking LOS communication, the RSSI was high whereas it was low on spots located next to trees.

On the other hand, the RSSI of the south leg of the intersection decreased from -54.54 to -90.02 dBm, in the distance range of 5 to 160 meters away from the RSU. It continued to decrease until it reached -109.7 dBm at 250 meters. Finally, for the east leg, no major change in the power was found whereas for the north leg, the RSSI for the whole leg length was -109.9 dBm with a corresponding PDR of 0%. The reason for the last two observation is that the LOS communication was unobstructed in the east leg whereas the north leg had a large tree blocking the LOS communication.
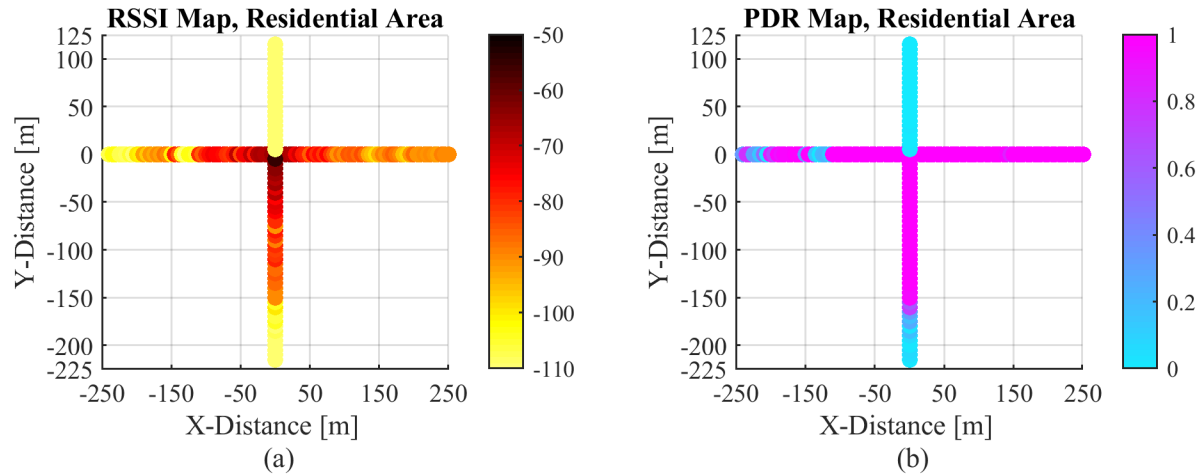
Figure 2.3 Received signal metrics for the residential area.
(a) RSSI map (b) PDR map

Figure 2.4a and 2.4b show the RSSI and PDR contour maps, respectively, for the commercial intersection. The RSSI of the west leg has decreased gradually for the whole leg length from -64.80 to -98.54 dBm. The RSSI of the east leg started from -75.04 and reached -100.21 starting from a distance of 5.0 meters up to 210.0 meters. In the north leg, the RSSI and PDR were almost constant with no significant changes. Finally, the RSSI of the south leg had a constant power of -70.46 and PDR of 98.56% up to a leg length of 250 meters. The change in results from the middle of the intersection to the north leg is so abrupt might be attributed to the obstructions found in the residential area.

Figure 2.5a and 2.5b show the RSSI and PDR contour maps, respectively, for the rural intersection. The RSSI of the north leg, has decreased from -53.92 to -103.72dBm between the distances of 10.0 and 240.0 meters and the corresponding PDR decreased from 99% to 75%. Between 240.0 and 250.0 meters, the RSSI dropped to -104.16 dBm with a corresponding PDR of 68%, and then the RSSI started to increase again between 250.0 and 500.0 meters, the PDR went up to 99%. This happens due to the region's topography (shadowing effects). To elaborate, the rural areas are located on the rolling hills of the Palouse and at times, the roads although straight, have sharp dips and rises.

The RSSI of the south leg decreased steadily (from -68 to -100 dBm) up to a distance of 220.0 meters, and then the range of RSSI dipped sharply to within the range of -109.38 to -109.51 dBm from a distance of 220 meters up to 260 meters. The range of the corresponding PDR fell sharply to within the range of 67% to 59%. This occurred due to road curvature and dip at that specific section. From 260.0 to 500.0 meters, the RSSI was higher again with a received power of -

96.8 dBm corresponding to a PDR of 92%. Finally, in the east leg, the RSSI decreased slightly between 10 and 240 meters in the range of (-63, 109) dBm corresponding to a PDR in the range of (99.9, 36.0) %, and between 240.0 and 500.0 meters the RSSI range was -109.45 to -110dBm with the PDR nearly zero.

The contour maps depicting the RSSI and PDRs at different distances from the RSU are important to visualize the communication behavior. One can observe, at the same distance from the RSU towards the north in the rural area that the received power is higher compared to the residential area. The reason is that there are wide areas of uninterrupted service in the rural region as compared to the suburban area where there are light poles and large trees blocking the LOS transmission. However, the common theme is that the PDR changes according to the RSSI. In other words, in both cases, the PDR appears to be a function of the RSSI and not of the environment or distance. This premise forms the basis for predicting the impact of these parameters on the RSSI to estimate the PDR.

(a) (b)
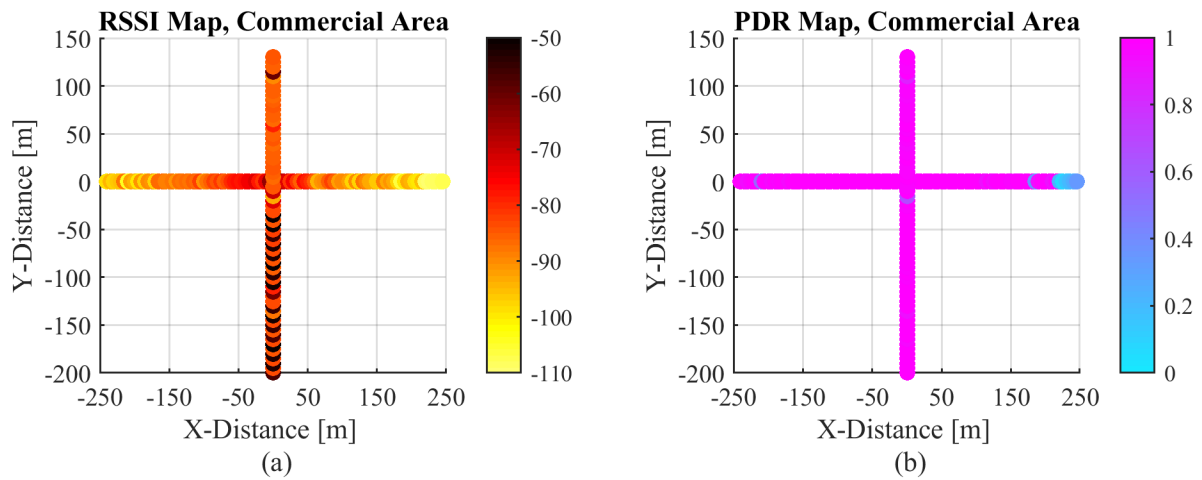
Figure 2.4 Received signal metrics for the commercial area.
(a) RSSI map (b) PDR map
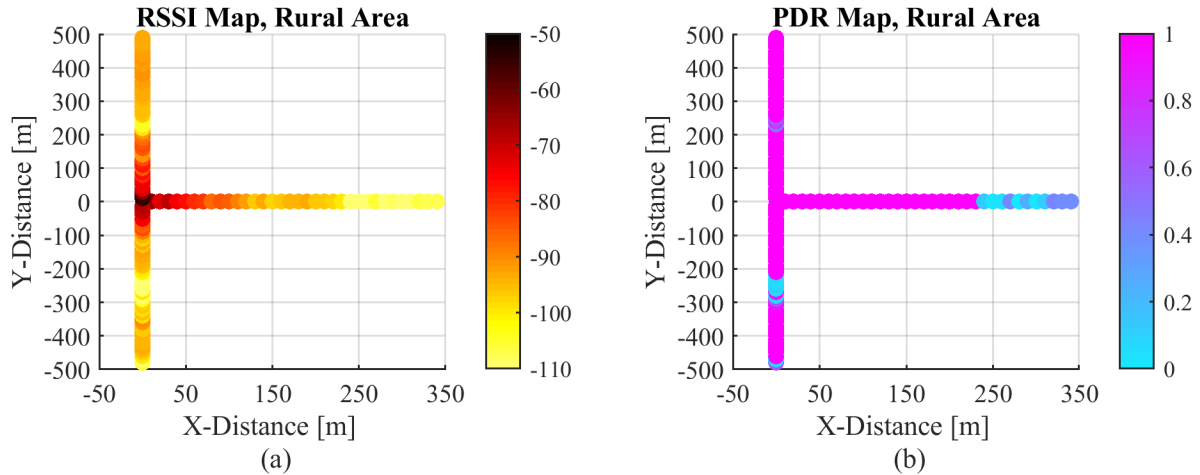
Figure 2.5 Received signal metrics for the rural area.
(a) RSSI map (b) PDR map

2.4.3 Mobile Test Results

Statistical data binning was used to group continuous values into a smaller number of "bins". The data for each trip (0.5-mile-long) was binned for 10 points (0.05 mile for each bin). Points were extracted from the data based on the time stamps. For instance, for the 10 mph condition, the width of the bins (in seconds) was calculated by the following operation: 0.05 mile/0.00278 mile per second = 17.98 seconds. To illustrate further, the bins for the tests at a speed of 20 mph were calculated by the following way: 0.05 mile/0.00556 mile per second = 9 seconds. The RSSI and PDR were calculated for each bin using the same procedures described in Equations (2.1) to (2.5).

Similar to the static test, 80% of the data points were considered for training, and 20% of the data points were considered for testing. The regression model used in the mobile test is described in Equation (2.6). Figures 2.6-2.9 show all the measured data points (training and testing) for speeds of 10, 20, 30, and 40 mph, respectively. For each speed, the regression model was used to fit the trained data and then the test data was used to validate the regression model for each speed test as shown in Figures 2.6-2.9 (a). The same process was followed for all speeds, where the training/fitting results for each of the respective speeds of 10, 20, 30, and 40 mph are displayed in Figures 2.6-2.9 (b). The testing performance is shown in Figures 2.6-2.9 (c).
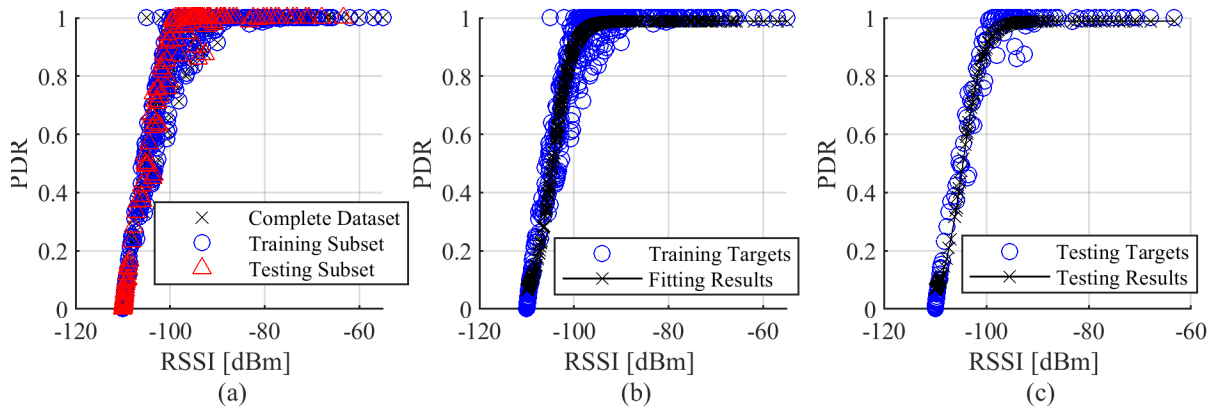
Figure 2.6 Complete data for 10 mph speed.
(a) Train/Test split illustration (b) Training results (c) Testing results
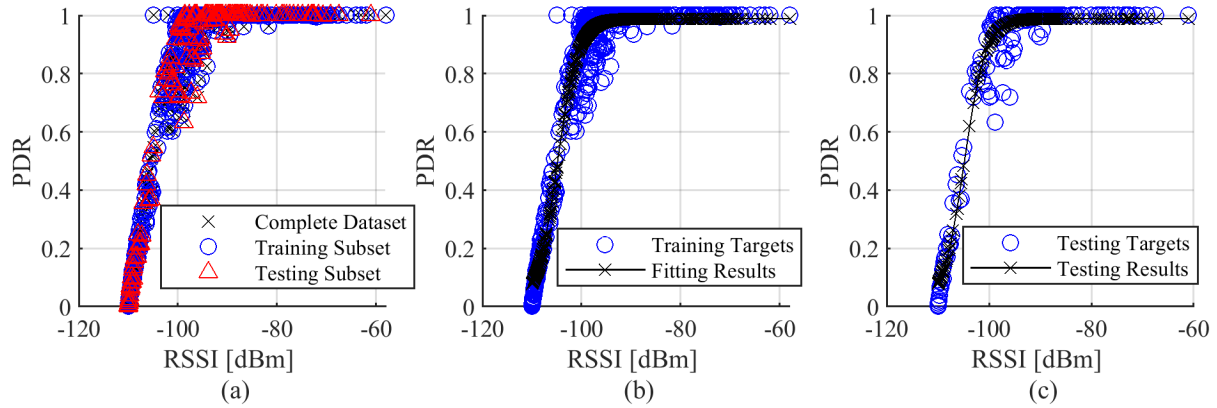
Figure 2.7 Complete data for 20 mph speed.
(a) Train/Test split illustration (b) Training results (c) Testing results
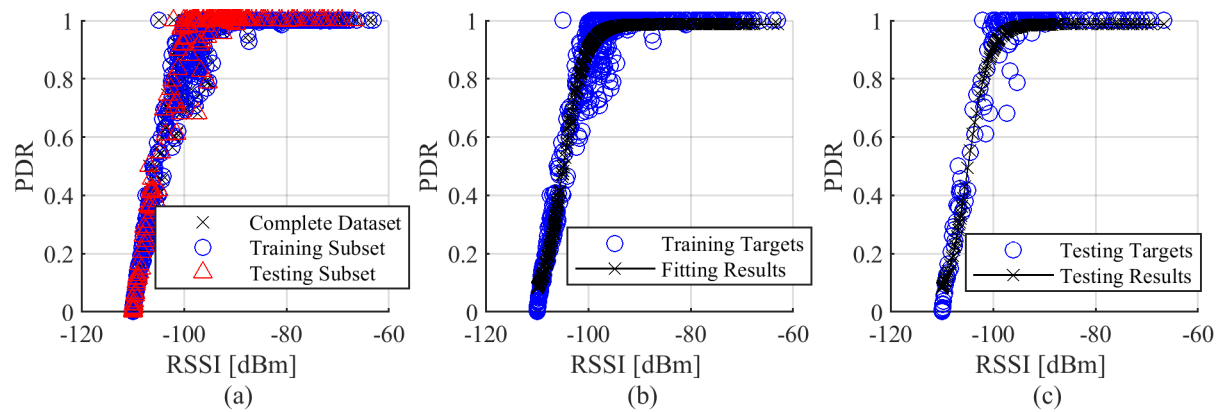
Figure 2.8 Complete data for 30 mph speed.
(a) Train/Test split illustration (b) Training results (c) Testing results
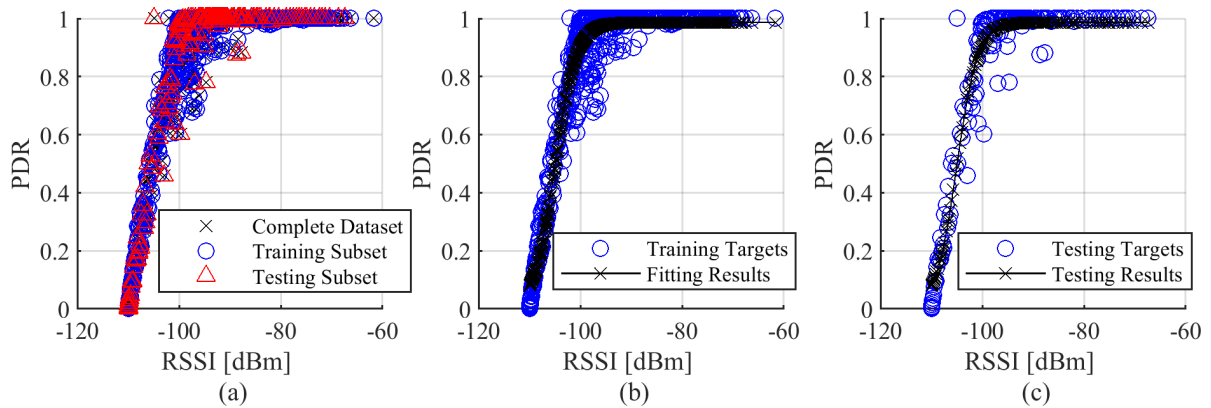
Figure 2.9 Complete data for 40 mph speed.
(a) Train/Test split illustration (b) Training results (c) Testing results

The statistical analysis shows that the variance of the validated data (tested data) at 10 mph was the lowest with RMSE of 5.2% and R^2 of 98.5% and the highest variance occurred when the speed was 40 mph with RMSE of 7.2% and of R^2 of 96%. For speeds 20 and 30 mph, the variance was almost the same with RMSE of 6.2% and R^2 of 97%. In general, the variance increased slightly with increasing the speed. When all the speeds were compiled together, the analysis showed that the variance of all speeds (RMSE of 6.1% with R^2 of 98%) was very close to the average variance resulting from the tests of each individual speed. The statistical summary of the trained data versus the testing data for different speeds is presented in Table 2.3.

The logistic model curve comprises of three different zones (linear, transition and saturation). Looking more closely at this curve, it was found that the variance of the saturation zone for the 10-mph speed was the lowest (1.0%), where the highest was attributed to the 40-mph speed (3.3%). For the transition zone, the variance did not follow a well-defined trend as shown in Table 2.4. Finally, the linear zone variance was observed to increase as the speed increases except at the highest speed of 40 mph. Overall, the highest accuracy was seen in the saturation zone followed by the linear zone. The transition zone had the lowest accuracy as shown in Table 2.4.

Table 2.3 Statistical summary of the trained data versus the test data for the mobile test

Variables	Speed 10 mph		Speed 20 mph		Speed 30 mph		Speed 40 mph	
	Calibration	Validation	Calibration	Validation	Calibration	Validation	Calibration	Validation
	(Train data)	(Test Data)	(Train data)	(Test Data)	(Train data)	(Test Data)	(Train data)	(Test Data)
N sample	623	154	620	154	662	164	693	172
Q	0.988	0.988	0.988	0.988	0.986	0.986	0.986	0.986
α	0.496	0.496	0.476	0.476	0.477	0.477	0.486	0.486
β	-104.62	-104.62	-104.85	-104.85	-104.91	-104.91	-104.99	-104.99
RMES (%)	6.48	5.19	6.00	6.24	6.16	6.24	6.16	7.20
R^2	0.98	0.99	0.97	0.97	0.97	0.97	0.97	0.96

Table 2.4 Statistical summary of the logistic zones for the mobile test

Vari.	Speed 10 mph			Speed 20 mph			Speed 30 mph			Speed 40 mph		
	L^*	T^*	S^*	L^*	T^*	S^*	L^*	T^*	S^*	L^*	T^*	S^*
RMSE%	5.50	5.80	1.00	5.80	9.10	1.70	7.10	8.80	1.40	6.30	11.00	3.30
R^2	0.860	0.939	1.000	0.920	0.317	1.000	0.884	0.624	0.999	0.932	0.481	0.999
	Overall data			Overall data			Overall data			Overall data		
RMSE%	5.2			6.2			6.2			7.2		
R^2	0.985			0.971			0.972			0.960		

*L=linear, T=transition, and S=saturation

Notice that the variance among the model parameters is very low. Once again, as we conclude from the contour plots in Figures 2.3-2.5, the PDR is a function of the RSSI. Varying speeds will impact the RSSI as fast fading occurs due to doppler effects. However, the quantity that impacts the PDR directly is the received signal power. This is also visible from Figure 2.10 which shows that collating PDR versus RSSI data collected at different speeds gives a scatter plot that is similar to the stationary experiments.

A more detailed analysis was also performed for all PDR values associated with each of the zones described above and the corresponding RSSI values. The reliability of V2I under different types of traffic conditions was investigated and it was discovered that the strength of V2I signals cover up to 1640.42 ft., which is more than the designed distance of signalized intersections in urban

corridors. Table 2.5 shows that the RSSI values for each zone for all speeds at the low power were around -110 dBm which is associated with PDR of 0.0%. On the other hand, the RSSI values at the high power were around -66 dBm with a corresponding PDR of 100%. For all speed tests, when the received power decreases from -104 to -110 dBm, a sharp linear drop of PDR occurs (on average 50% to 0.0%). In the transition zone, when the average RSSI power decreases from -93.75 to around -104 dBm, the average PDR dropped from 98.24% to 50%. In the saturation zone, when the RSSI average decreases from -65 to around -93.75 dBm, the average PDR dropped very slightly from 100% to 98.24%.

Table 2.5 RSSI range vs. PDR for the mobile test

Speed 10 mph		Speed 20 mph		Speed 30 mph		Speed 40 mph	
RSSI	**PDR**	**RSSI**	**PDR**	**RSSI**	**PDR**	**RSSI**	**PDR**
-63.28→ -90	100%→ 98.99	-61→ -93	100%→ 98.99	-66→ -95	100%→ 96%	-67→ -97	100%→ 98.99
-90→ -104.61	98.99%→ 60%	-93→ -104.85	98.99%→ 50%	-95→ -104.90	96%→ 49%	-97→ -104.98	98.99%→ 43%
-104.61→ -110	60%→ 0%	-104.85→ -110	50%→ 0%	-104.90→ -110	49%→ 0%	-104.98→ -110	43%→ 0%

Figure 2.10 Training/testing split of the complete dataset at all speeds (10-40 mph).
PDR versus RSSI and subsequent fitting/testing results using a logistic model. (a) The complete dataset with
train/test split (b) Logistic Model fitted/trained data (c) Tested data with the calibrated regression model.

2.5 Correlation between RSSI Measured from the Vendor Tool and the Power Meter

The correlation between the power meter and the dedicated tool was found to be on the higher side (r =+0.81) which is positive. The p-value of the paired sample t-test (a.k.a. the dependent sample t-test) was 0.330 (which is statistically not significant). Moreover, the confidence interval (CI) was calculated for both, the power meter and vendor-supplied tool readings to check if they comprise the close-range values that contain the true mean of population of readings. The average mean for the vendor-supplied tool was -83.15 dBm and for power meter was -82.18 dBm. The margins of error for the power meter readings were 3.27 dBm, 3.74 dBm, 4.45 dBm and 5.86 dBm for 85%, 90%, 95%, and 99% CI, respectively. The margins of error for tool reading were 2.11, 2.42, 2.76 and 3.79 for 85%, 90%, 95%, and 99% CI, respectively. Therefore, we can conclude that the differences in readings between the vendor tool and the power meter were low except for one outlier.

A linear regression model was developed to fit the data between the two tools as shown in Figure 2.11. Let the power measured using the RF meter be denoted by $RSSI_m$ and the power reported

by the vendor tool as $RSSI_m$, where $RSSI_m$ and $RSSI_v$ are represented by x and y, respectively, in Figure 2.11. Then, the RSSI from the vendor can be related to the measured RSSI using the linear relation given by:
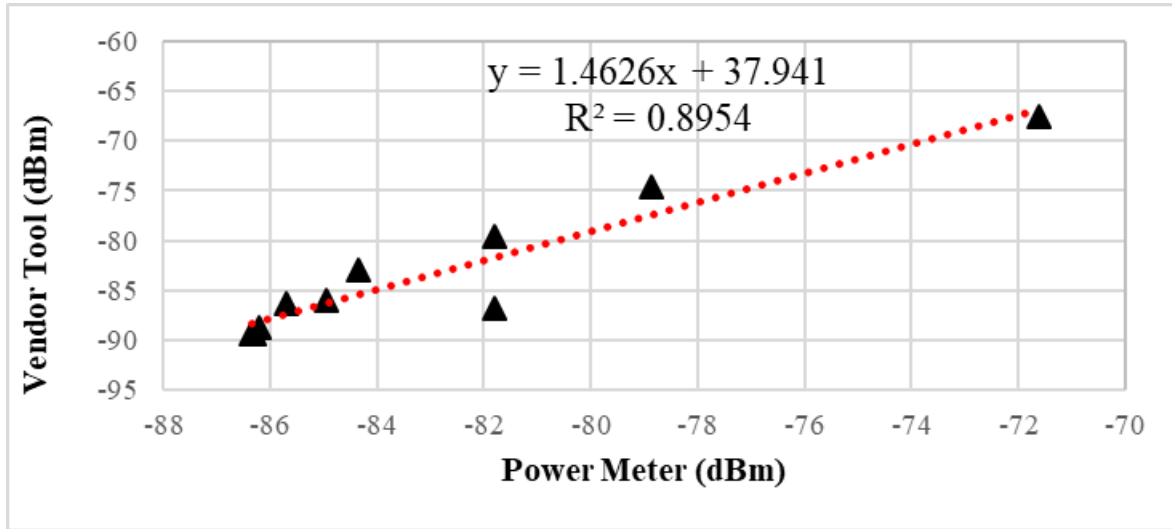
Figure 2.11 Vendor Tool vs Power Meter (linear regression)

$$RSSI_v = 1.4626 RSSI_m + 37.941\ [dBm] \tag{2.7}$$

The resulting models' R^2 was 0.89 and RMSE was 2.21%. Based on that, we can conclude that the power meter can be used as an independent tool to measure the PDR of this vendor's RSU using the developed logistic model with high confidence assuming that the noise floor ranges between -86 and -70 dBm. The model may also be used as is for other vendors' RSU's. The details of how to extend this work to other models are provided in the conclusion. Moreover, the low power range correlation could be forecasted based on the hypotheses developed in this study.

2.6 Case Study

The research team visited two signalized traffic intersections in Boise, Idaho (Figure 2.12), where RSU's from two vendors (A and B) were installed. The team used the power meter to measure the RSSI from the different RSU's installed at the two intersections of W Franklin Rd with N Liberty St (urban corridor) and E Franklin Rd with S Touchmark Way (suburban corridor). The data collected were based on static tests where the team collected the readings by stopping at each predefined station and recording the readings. The PDR could be predicted using the linear regression model developed earlier in Equation (2.7) (between the power meter reading and the dedicated vendor-supplied tool).

In other words, the RSSI was obtained using Equation (2.7) and the resulting RSSI was substituted back in Equation (2.6) to estimate the PDR. The parameters used in the estimations were obtained from the previous analysis as shown in Equations (2.8) and (2.9), for stationary and moving readings, respectively.

$$E(PDR) = \frac{0.9953}{1 + e^{(-0.7019x - 68.4836)}} \tag{2.8}$$

$$E(PDR) = \frac{0.9953}{1 + e^{(-0.6989x - 68.189)}} \tag{2.9}$$

(a)   (b)

Figure 2.12 Aerial view of the two intersections considered for testing in Boise, Idaho.
(a) Intersection 1: E Franklin RD with S Touchmark way (b) Intersection 2: W Franklin RD with N Liberty St. Boise ID

The benefit of using our model is that the performance of equipment from various RSU/OBU vendors can analyzed via independent tools (power meters) without deeply investigating the RSU software. Thus, DOTs can evaluate the PDR data obtained from RSU vendors without relying on their provided software/tools, which allows them to independently assess coverage reliability of connected vehicle signals under different conditions. Figures 2.13 and 2.14 show the RSSI and PDR contour maps for vendor A and B, respectively. The range of RSSI readings was from -50 to -73 dBm and the PDR was between 99.9% to 99.7% for both vendors.
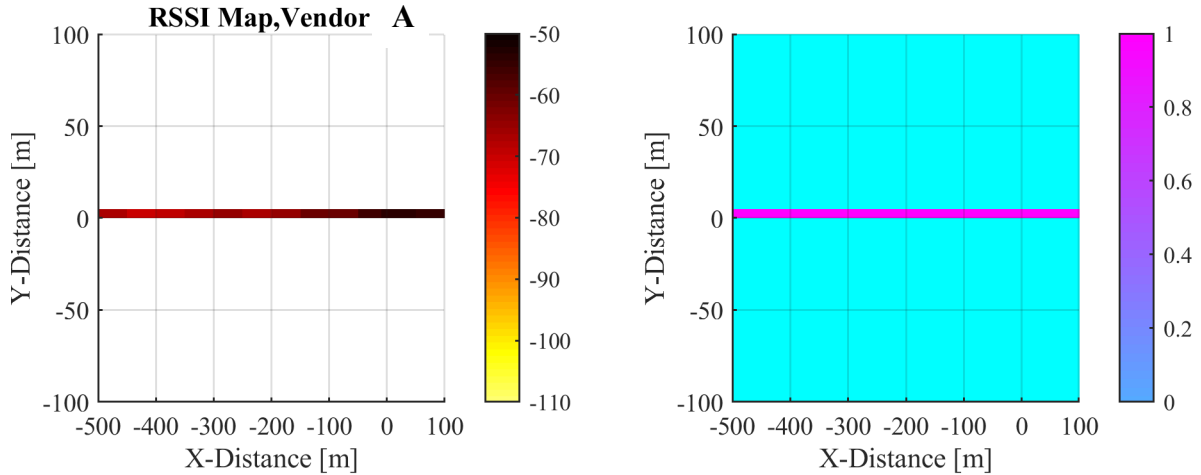
Figure 2.13 Vendor A RSSI and PDR maps at Boise intersection 1.
(a) RSSI map (b) PDR map
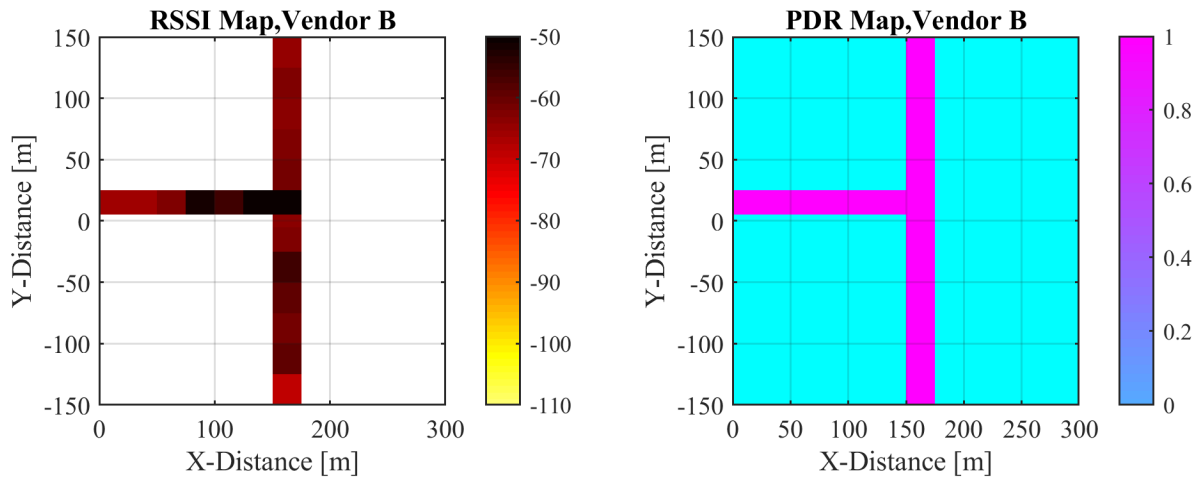
Figure 2.14 Vendor B RSSI and PDR maps at Boise intersection 2.
(a) RSSI map (b) PDR map

2.7 Conclusions

This study developed a vendor-independent reliability model for testing the communication reliability of V2I communications. The tests were conducted at three different types of traffic intersections with the RSU fixed at a height comparable to a traffic light pole and the OBU placed inside a vehicle. For one of the vendors, both the RSSI and PDR were measured as a function of the LOS distance of the OBU from the RSU, using the vendor's tool. This was followed by independent measurements of the RSSI using an RF power meter. A logistic expression was derived to relate the PDR to the vendor reported RSSI. A linear regression model was then developed to fit the data between the vendor tool and the independent power meter. The best derived model gave an R^2 of 89%

and an RMSE equal to 2.21%. The result was an expression for the PDR as a function of the measured RSSI. The developed statistical models have been used in a case study in two actual intersections in Boise, Idaho to evaluate the efficiency of two vendors' RSU.

One important conclusion of this work is the repeatability to other vendors' equipment, environments, and types of intersections. As described, there are two aspects to these results, linking the PDR to RSSI and correlating measured RSSI with vendor reported RSSI. It is expected that the PDR would perform similar to the reported results versus RSSI because the underlying physical layer communication is implemented according to the DSRC standard; the discrepancies are in the higher layers of the network (e.g., data link, network and application layers). However, the RSSI may vary among different vendors and may vary slightly with different power meters. Therefore, for any agency to reproduce our results, they may have to correlate the RSSI reported by both, their meters and RSU's or they may even need to develop a generalized model by collecting results from multiple meters and RSUs.

The value our work is in the fact that it demonstrates how agencies only need to correlate the RSSI of their independent meters to vendor tools which does not require live field testing, only a testing setup that will ensure signals are received from low ranges of power to high power. Once this correlation is done, the PDR can be estimated as a function of RSSI. Overall, the results of this study provide a valuable independent technique for transportation agencies and USDOT to evaluate the efficiency of any RSU vendors' performance without accessing the specific vendors' software.

Chapter 3: Analysis of Heavy Vehicle Wind Force on Cyclists

Madkour, Fatma Elzahraa, Michael Lowry, Ahmed Abdel-Rahim, Durgesh Vibhav, and Yu Paulo Analysis of Heavy Vehicle Wind Forces on Cyclists" Submitted to Transportation Research Records.

3.1 Introduction

The National Highway Traffic Safety Administration (NHTSA) has reported roughly 800 cyclist fatalities per year from motor vehicle crashes for the past three years. NHTSA reported an increase of 32% of pedestrian and cyclist fatalities between 2008 and 2017. The medical expenses of fatal and non-fatal cyclist crashes were \$28B and \$209B from 1999 to 2013 [1]. In rural areas, cyclist often ride on two lane highways for recreation and for intracity travel. Cyclists in rural areas who overtaken by vehicles is not fully investigated.

There are many cases where cyclists being hit by the wind created by passing vehicles and trucks, where it was reported by New York Police Department in 2016 that a cyclist was killed by an overtaken truck. However this unreliable proof has not been investigated before in the USA. Cyclists travel on rural areas at lower speeds compared to semi-trailer trucks and they usually have smaller shoulder width for maneuvering. The aerodynamic loads generated from moving vehicles trigger a concern on the stability and safety of cyclists which might lead to loss of control and consequently cyclist injury. The induced forces from passing trucks usually lead to instantaneous impact load on cyclists and this sudden force might affect their stability and lead to injuries. One of the reasons of this problem might be due to the limited transverse pavement shoulder spacing between a cyclist and the passing vehicle. The author realized the importance of investigating the effect of various vehicles, vehicle speeds, and separation distance on cyclist's immovability. The passing vehicles generate transverse forces (perpendicular to cyclist) and longitudinal forces (parallel to cyclists). The transverse forces produce flipping moments that might affect cyclist's stability. The results of this study will significantly help identifying various factors affecting safety of cyclists while in rural and urban areas. It is anticipated to develop various transverse force and moment levels that are generated from the passing vehicles and understand the characteristics of those forces and up to what level they affect the stability of cyclists on rural areas.

This study presents an analysis of the wind pressures/forces that are exerted on cyclists due to passing vehicles. The tasks of this research will be conducted experimentally by measuring the longitudinal and transverse wind speeds on a typical cyclist. The wind speeds induced from various vehicle types and separation distances at various vehicle speeds will be used to develop corresponding forces and flipping moments on cyclists and provide recommendations for cyclists' safety. In addition to the

field tests, numerical computer simulations were conducted to investigate the feasibility of predicting transverse and longitudinal forces on a typical cyclist. The computer simulations have included the same parameters of the field test such as vehicle type, and speed, and separation distances for the semi-trailer truck case. Finally, a 3D printed scaled (1:25) cyclist and semi-trailer truck models have been placed in a wind tunnel and the side and drag forces have been measured. Correlation between the computer simulations and the wind tunnel test will be presented. The overall trend of the experimental, computer simulations, and the wind tunnel will be investigated.

The generated wind speeds (transversely and longitudinally) by passing vehicles will be measured under various scenarios of vehicle speeds, separation distances and vehicle type. Those wind speeds will be used to calculate forces and moments based on the vehicle type and cyclist's characteristics, which will help to identify critical values of flipping moments that might affect stability of cyclists. The results of this study have been also compared to cited literature.

The goals of this study are to:

- Quantify wind speeds created by passing vehicles through real field tests, scaled computer simulations, and wind tunnel experiments.
- Determine the effect of varying vehicle speeds, and separation distances on force and flipping moment levels on a typical cyclist.
- Define the critical scenarios where separation distance and vehicle speed might affect cyclists' safety.
- Propose alternatives that might provide more safe environments for cyclists and to mitigate crashes.

This study defines factors affecting safety and stability levels on cyclists in a way that has not been done before. The Highway Safety Manual does not provide information related to this topic and the results will provide initial data to cover this gap.

The main tasks of this study were to perform, a) field tests to investigate the unsteady wind pressures generated by passing vehicles at various speeds and separation distances between the cyclist and the vehicle, b) A feasibility study of developing high-fidelity computational fluid dynamics (CFD) computer simulations to determine force levels on cyclists due to moving semi-trailer trucks at various speeds and separation distances. The field tests have been conducted using ultrasonic wind sensor (UWS) that was mounted at a height corresponding to the center of gravity of a typical cyclist. The results of the study will be used to develop recommendations and countermeasures of cyclist

safety on roadways, The results of the CFD were compared to a 3D printed semi-trailer truck and cyclist that have been tested under constant wind speeds generated from a wind tunnel test. The key parameters investigated were the relative speed between cyclist and truck (25, 40, and 60 mph), transverse spacing between cyclist and the truck (2 ft., 4 ft. and 6 ft.), and vehicle type (SUV, Pick-up truck, single unit truck and a semi-trailer truck).

3.2 Background

3.2.1 Wind Force Profile for Cyclists

Cyclists experience various forces, some of which translate into rotational moments that can be hazardous for their safety. The force profile on a cyclist consists of in-plane vertical and horizontal forces. The in-plane vertical forces are the gravity and normal forces which depends on the cyclist's weight and the friction between the bike and the ground surface, respectively. The in-plane horizontal forces are the drag (air resistance) and the thrust force from the cyclist. In the out-of-plane, cyclists usually have a transverse force (perpendicular to the side area of the cyclist), and flipping and rolling moments as shown in Figure 3.1.
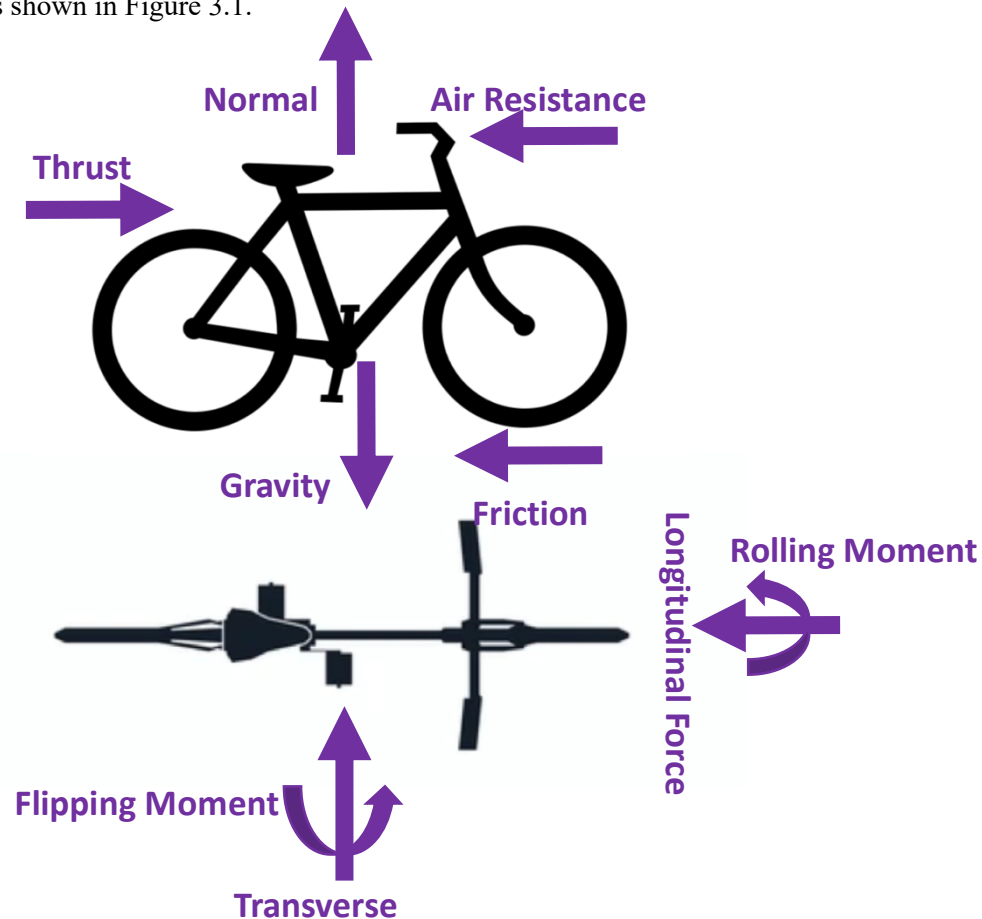

Figure 3.1 In-plane and out-of-plane force profile.

When a vehicle passes a cyclist, the vehicle generates wind forces that can negatively impact the cyclist's stability. In this study, the author focused on investigating two forces; the first is the transverse force that acts at the cyclist's center of gravity in the perpendicular direction of movement (Figure 3.1). The second force is the longitudinal force (drag force) that acts in the parallel direction of movement. This wind forces can arise natural, but significantly exasperated by passing vehicles. The magnitude of wind force from passing vehicles depends on vehicle speed, separation distance between the cyclist and the vehicle, and vehicle aerodynamics (vehicle type). Flipping and rolling moments are calculated by multiplying the force by the moment arm distance.

3.2.2 Literature review

This section summarizes the literature pertaining to forces induced on cyclists from passing vehicles. Ten studies were identified and obtained through an extensive search using Google Scholar and TRID (Transportation Research Information Database). Table 3.1 summarizes key aspects of the studies [2-11]. Previous studies on this topic are very limited and most of such work has been done in Europe (Germany) and almost none has been conducted in the USA. The previous studies have focused on sedan cars, pickups and one or two studies considered single unit trucks. To our knowledge there are no studies involving semi-trailer truck winds on cyclists, but rather quantifying wind forces exerted on overhead road signs. The key parameters studied include vehicle type, vehicle speed, separation distance with the passing vehicle, and also the cyclist riding position (upright or racing).

The FHWA [10] provided a tolerance limit for the transverse force on a cyclist of 3.82 lb. [17 N]. The source behind this limit is not provided and the underlying science behind this force calculation is not included in the publication. We note that FHWA [10] assumed the relationship between the passing truck speed and the force on the cyclist as linear functions, which might not be correct in all scenarios.

A few of the studies note that wider shoulders can help mitigate the impact of wind forces, unfortunately shoulder widths are often narrow on rural roads, especially in western states such as Idaho. Usually when a cyclist is exposed to sudden transverse force, the cyclist will try to adjust the bike position back to keep balance. This is valid when the transverse force is applied for a long period of time, so the cyclist has time to respond. The situation of sudden passing truck (60 mph) by a cyclist is totally different because the wind generated induces a sudden change in the transverse and longitudinal forces and that occurs in milliseconds. Because of the sudden change in the force, the cyclist has no time to respond. Those forces might produce loss of balance and lead to traumatic injury.

Table 3.1 Literature review summary

Author	Study goal	Location	Parameters considered	Methodology	Conclusions
Cali et al. (2000) [2]	Forces on road signs due to passing vehicles	USA-Experiments	Vehicle speed, length, shape, and sign height	Estimate of loads on road overhead signs using scaled (1:30) laboratory experiments.	• The highest load measured when the sign was on the opposite direction to the vehicle. • Forces measured depend on vehicle type
Quinn et al. (2001) [3]	Wind forces on flat plates	UK-Test Section	Sign size and road barrier size	Full scale instrumentation has been conducted on sign size of (750 mm - 1500 mm) Nondimensional analysis	• Sign size has no effect on the induced wind forces • Larger signs experience longer time of force exposure • The highest load measured when the sign was on the opposite direction to the vehicle
Sanz Andres et al. (2004) [4], Lee [11]	Forces induced on pedestrian due to passing trains	Spain-Theoretical	Train speed	Theoretical models have been developed to predict forces on pedestrians. Pedestrians have been modeled as cylindrical elements (no actual humans were involved).	Qualitative results have been obtained. Smaller separation distance results in larger forces. Forces mainly depend on the shape of the train and the shape of the cylinder (pedestrian).

Lichtneger et al. (2015) [5]	Field experiments on forces induced on road signs	Germany – Test Section	Sign size, vehicle type, and vehicle speed	Fully instrumented road signs have been exposed to various vehicle types and speed at various separation distances.	• Induced forces mainly depend on vehicle type and shape and separation distance. • The authors developed for the first-time characteristic load curves for each vehicle type.
Gromke et al.(2014) [6]	Aerodynamic loads on a cyclist while overtaking by a vehicle	Germany- Test Section	Passenger sedan car, Speed of 1.6 ft. to 6.6 ft. 0.5–2.0 m) and speed of 24.85 to 62.1 mph (40–100 km/h).	Fully instrumented dummy cyclist has been used to measure lateral forces on the cyclist at various speeds (40 to 100 km/h) and separation distances (0.5 and 2.0 m). The test has been done at a controlled test section.	• The authors present the side force rate was introduced and correlated to the passing distance, and the car speed. • The force-time history measured between the vehicle and the cyclist showed a pressure and a suction phase that exerted on a cyclist at the moment a car passes by a cyclist at a certain speed. The flip over (lateral force) on a cyclist was in the range of 0.5 N to 31.1 N that corresponding to a duration range of 0.07s to 0.24s
Lubitz et al. (2018) [7]	Investigate transverse forces on cyclist due to pick-up truck and develop flipping moment diagrams.	Canada- Test Section	Pick-up truck, separation distance, vehicle speed	Conducted experiments on a full-scale dummy cyclist to measure lateral forces induced from passing pickup truck (2001 Dodge Ram).	• The authors have measured both forces and wind speeds. • The forces were linked to the measured wind pressure, however the measured speeds were in the magnitude of 1 m/s.

					The authors developed an equation to calculate flipping moment. they suggested that measuring wind speed is enough and sufficient in future experiments to investigate the longitudinal and lateral forces exerted on a cyclist from a passing truck.

Author	Study goal	Location	Parameters considered	Methodology	• Conclusions
Walton et al. (2005) [8]	Quantify lateral and longitudinal forces on cyclists induced by passing trucks	New Zealand- Test Section	Single unit truck 42.6 ft. (13 m), separation distance of 1.6 ft., 3.3 ft., 4.92 ft., 6.6 ft., 9.84 ft. (0.5, 1, 1.5, 2, and 3 m), and truck speed 18.6 mph, 31 mph, 43,5 mph, 49.7 mph, (30, 50, 70 and 80 km/h).	Two anemometers have been placed at a rural highway and the wind generated from traffic was recorded.	• The authors observed that the passing truck generates a wind pulse in the lateral direction • At the beginning, the pulse direction was away from the vehicle and then it changed its direction towards the vehicle. In addition, as truck speed increases, time duration decreases, and wind pressure increase. • At higher speeds, the truck induced an impulse force of 22.48 lb. (100 N) hit the cyclist from the back, which might affect cyclist instability. At higher speeds, the truck induced an impulse force of 22.48 lb. (100 N) hit the cyclist from the back.
Llorca et al. (2017) [9]	Find a correlation between vehicle speed, separation distance and risk on cyclists.	Spain- 7 rural roads. Test Section	Various vehicle types, separation distances, and speeds	Two real cyclists were instrumented with sensors and cameras used to record actual separation distance and vehicles' speed.	• The separation distance was not the only factor influence cyclist reaction. • Heavy vehicle had a significant effect on cyclists. The correlation between separation distance, vehicle type and speed were significant factors to be considered on cyclists' safety.

3.3 Methods

This section describes the overall methodology used to achieve the study tasks. The goal was to identify the forces exerted on cyclists due to various vehicle types, vehicle speed, and separation distance between the cyclist and the passing vehicle. The first part of the data collection was conducted using real field tests with real vehicles. The instrumentation used will be described next. The second part of the study involved analysis using computational fluid dynamics (CFD). The third part of the study involved creating physical models of a scaled (1:25) truck and cyclist and observing forces generated in a wind tunnel. The physical models were designed using standard semitrailer truck dimensions available in the literature [12]. The truck dimensions were scaled and printed with a 3-D printer at the Mechanical Engineering Department at the University of Idaho. The goal of using CFD models and physical models was to investigate the feasibility of quantifying forces on cyclists using computer simulations and wind tunnel experiments and to correlate the overall behavior with the observed forces from the field.

3.3.1 Field Tests in Controlled and Uncontrolled Environments

A stationary instrumented 3-D ultrasonic wind sensor (UWS) was placed at the shoulder area of roadway and highway sections in Moscow, ID to measure the longitudinal and transverse wind speeds generated from vehicles' movement. The wind sensor was located in three positions (three separating distances) from the test vehicle path. The test vehicle traveled with various speeds as will be discussed next. The UWS was mounted at height of 4 ft. from the ground surface (centroid height of a typical cyclist). The field tests were done in controlled (road with no traffic besides the test vehicles) and uncontrolled environments (highway section with natural traffic flow). The measurements were taken on very similar days in terms of ambient wind speeds and temperature. The distance between the vehicle passing and the UWS was measured directly by making marks on the asphalt where the driver tried to follow the path. The actual separation distances were recorded, and the accuracy was in the range of ∓ 5 inch. The UWS has been connected to the CR6 datalogger and a laptop (Figure 3.2). The data was collected using Logger Net software that is compatible with the CR6 datalogger. The logger was able to record and store the data every 100 millisecond at a sampling rate of 20 Hz. The UWS and the data logger were set to voltage output which converted to corresponding wind speeds in m/s based on the calibration factors of the UWS. The separating distance was based on the distance from the center line of the cyclist and the side of the test vehicle.

The UWS YOUNG Model 86000 was used in this study. This UWS is relatively small compared to old wind anemometers and is supported with advanced technology that offers high measurement

sensitivity (Figure 3.2). All the specs of the 86000 sensors are shown in Appendix A. This sensor could read wind speeds in two perpendicular directions (parallel and perpendicular to traffic direction).

Figure 3.2 Test setup and UWS (Young 86000 anemometer).

The main goal of this task was to investigate the longitudinal and transverse wind speeds experienced by cyclists from various moving vehicles and separation distances and vehicle speeds. This section presents a full description of the instrumentation, test vehicles and the overall methodology of the field tests.

The field test was conducted under two conditions described as follows:

   a) Controlled Test

In the controlled test, a rural specific test section was chosen in Moscow, Idaho (Figure 3.3). The test section has very low traffic volume, which minimizes other vehicle's interference to the data collected. This test was controlled because the speed of the tested vehicle and the separation distance were under control. Under the controlled test, four vehicles (SUV, Pickup truck, Single unit truck and semitrailer truck) were chosen to represent all different traffic volumes.
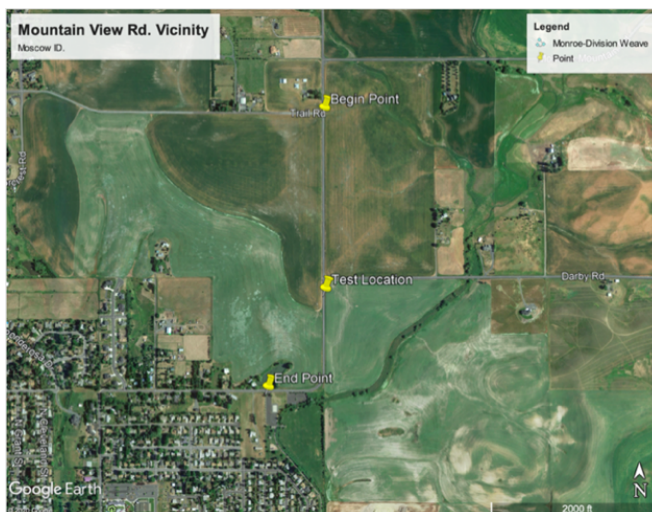
Figure 3.3 Test section

The four vehicles were an SUV (2010 Toyota highlander), pickup truck (2020 Dodge Ram 1500), single unit truck (ford hauler) and finally a 5-axle semi-trailer truck (Freightliner), (Figure 3.4). The FHWA did not report any vehicle related information that support the force on cyclist threshold value. Table 3.2 shows the dimensions and the frontal area of the four vehicles used in all tests. Figure 3.4 shows the four vehicles while performing the field tests. The side length and side cross sectional areas were not included because they do not contribute to the forces or flipping moment generated by overtaken vehicle.

Table 3.2 Vehicles' characteristics

Vehicle	SUV- 2010 Toyota Highlander	Pickup Truck- 2020 Dodge Ram 1500	Single Unit Truck-Ford	Semitrailer- Freightliner 5- axles
Frontal Area, ft² (m²)	35.56 (3.03)	44.24 (4.11)	67.37 (6.26)	96.4 (8.96)
Drag Coefficient	0.340	0.357	0.80	0.80
Gross Vehicle Weight, lb. (kg)	6,000 (2,721.5)	6,900 (3,129.78)	25,999 (11,792.948)	80,000 (36,287.4)

(a) SUV

(b) Pickup Truck

(c) Single unit truck

(d) Semitrailer Truck

Figure 3.4 Vehicles used in the controlled test.

Each test case was repeated 5 times which resulted in a 194 data points. Some trials were repeated 6 times instead of 5 where the author felt some malfunction of the system. The driver tried to maintain the required distance between the side of the vehicle and the centerline of the wind sensor, and that was achieved by making marks on the road as shown in Figure 3.5. The exact separation distance was measured using a laser meter where the actual distance variance was $\pm$ 5 inches. In addition, the driver-maintained vehicle speeds constant and accurate (using cruise control) for the 200 feet before and 200 feet following the position of the UWS. The test trials were performed under dry weather conditions. All measurements were recorded during moderate wind conditions of about 2.2 to 3.4 mph (1 to 1.5 m/s) above ground. The studied parameters were vehicle types, speed limit, separation distance between the cyclist and the overtaking vehicle, and the cyclist types. Three cyclist positions have been cited from [5] and used in this study as shown in Table 3.3. The three positions helped in identifying the force and flipping over moments affecting such cyclists' scenarios. Table 3.3 shows the field test matrix.

Figure 3.5 Location of marks on pavement for various side distances.

Table 3.3 Field Test parameters

Vehicle Speed, mph (m/s)	Designed Separating Distance, ft. (m)	Vehicle type	Cyclist Types [5]
25 (11.17)	2 (0.61)	Semi-trailer Truck	Adult on a touring bike (As=0.94 m^2)
40 (17.88)	4 (1.22)	Semi-trailer Truck	
60 (26.82)	6 (1.82)	Semi-trailer Truck	
25 (11.17)	2 (0.61)	Single Unit Truck	
40 (17.88)	4 (1.22)	Single Unit Truck	Adult on a touring bike with front and rear wheel saddlebags (As=1.14 m^2)
60 (26.82)	6 (1.82)	Single Unit Truck	
25 (11.17)	2 (0.61)	SUV	
40 (17.88)	4 (1.22)	SUV	
60 (26.82)	6 (1.82)	SUV	Adult on a racing bike (As=0.79 m^2)
25 (11.17)	2 (0.61)	Pickup Truck	
40 (17.88)	4 (1.22)	Pickup Truck	
60 (26.82)	6 (1.82)	Pickup Truck	

*As= side area of a cyclist

b) Uncontrolled test

For the uncontrolled test, the wind speed measurements were recorded under real traffic volumes. The data was collected from US 95 under three different speed limit segments of 25 mph, 45 mph and 65 mph (11.17, 17.88, and 26.82 m/s). The instrumentation was placed at the exact separation distance similar to the controlled test of 2 ft., 4 ft, and 6 ft. (0.61, 1.22, and 1.82 m). The data was collected for the same types of vehicles used under the controlled test. The data from the uncontrolled test was to validate the results obtained from the controlled test. A speed gun was used to catch the actual vehicles speeds. One of the challenges in this uncontrolled test was noticed when drivers change lanes when they see the instrumentation and some of the drivers started to drive away from the instruments or reduce their speeds. Therefore, we had a real cyclist in the test section to be able to have accurate results compared to the controlled section. Figure 3.6 shows a snapshot of a semitrailer passing by the instrumentation.

Figure 3.6 Snapshot of a semitrailer truck passing by the instrument.

3.3.2 Computational Fluid Dynamics Simulations

The second part of this study involved using high-fidelity computational fluid dynamics (CFD) simulations to model the complexity of cyclists and truck geometry. The CFD is a Powerful tool that could be used to investigate any further cyclists' behavior by overtaken trucks. The truck and cyclist models have hundreds of details that have been included with some assumptions. For example, the details of the bile such as the wheel spokes, cyclist head and hands, etc. This approach is a novel research method and has not been done to the author's knowledge.

This section presents the procedure of developing the CFD simulations, where they are very computationally expensive. The semi-trailer truck and the cyclist were scaled down to 1:25 to be able to perform the simulation with the available computational resources.

The performed simulations have built up with very fine mesh (6+ million nodes) and the method of Improved Delayed Detached Eddy Simulation (IDDES) turbulence model was used [11]. IDDES is a crossbreed model that precisely solve complicated flow problems such as the interaction between the semi-trailer and cyclist problem without compromising other aspects such as boundaries 'separation.

    a) Geometry Description of Semitrailer-truck and Cyclist Geometry

A generic semi-truck model was chosen from the common federal highway administration website (US truck fleet). It is a 5-axle truck with gross vehicle weight of 80,000 lb., as shown in Figure 3.7.

The semi-trailer truck (Figure 3.7) was a Freightliner with trailer attached to the main cab. The total length was 53 ft. (16.15 m) semi-trailer with five axles. The CFD model has been generated with solid parts where wheel openings, windows, front grill, side mirrors, and wheel wells were ignored in the simulations. This simplification also rationalized the CFD mesh production process.
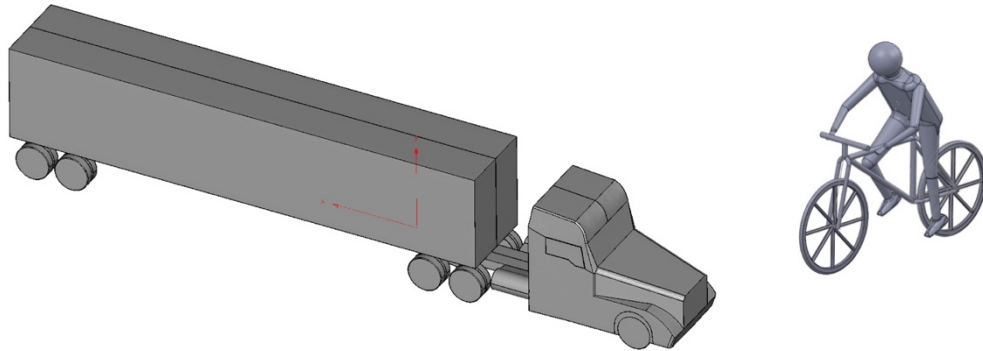

Figure 3.7 Geometry of the scaled truck and the cyclist (not to scale)

The cyclist was modeled based on a typical biker with upright position and was assumed to behave as a rigid body in all the simulation performed. The model was designed to represent a typical cyclist in terms of the length, and overall height. The details of the biker were included as shown in Figure 3.7. Table 3.4 shows the cyclist and the scaled truck dimensions used in all the simulations.

Table 3.4 Cyclist and the semitrailer truck scaled dimensions

Dimensions	Cyclist	Semi-trailer truck
Length, inch (mm)	3.16 (80.16)	32.69 (830.54)
Width inch (mm)	0.82 (20.84)	3.94 (100.02)
Height inch (mm)	2.40 (60.84)	6.32 (160.44)
Frontal Area, in.^{2}(mm^2)	1.97 (1267.91)	24.9 (16047.21)

b) Mesh Generation

The dimensions of the cyclist and the semitrailer truck were scaled to 1:25 to be validated experimentally through wind tunnel testing. The commercial software PointWise was used to produce the cyclist and truck's mesh where the elements mesh generation was assumed the same for all bodies (cyclist and truck). The un-structured option was implemented in the meshing process, while the fluid volume (air) was engulfing the cyclist and the truck was produced using a structured mesh. The volume of air around the truck and the cyclist was generated with un-structured triangular elements. The air in front and behind the truck was modeled as well, and it was called the dynamic

mesh zone and modeled with a structured mesh. Figure 3.8 shows a cross section of the mesh that was used in the modeling. The zones were structured with very fine cubical mesh (higher resolution), where their sizes were 0.4×0.4×0.4 mm.
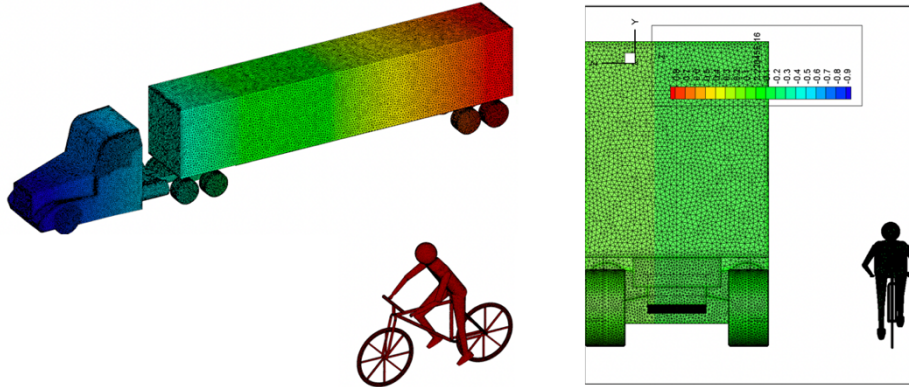
Figure 3.8 Truck and bike mesh

In all simulation of cyclists versus moving trucks, the cyclist was assumed stationary, and the semitrailer truck was assumed moving with a speed that matches rural roads' speed limit. Speeds of 25, 40, and 60 mph (11.17, 17.88, and 26.82 m/s) were considered in the simulations. The simulation matrix is shown in Table 3.5, while Figure 3.9 shows the overall domain used for the truck and the cyclist.
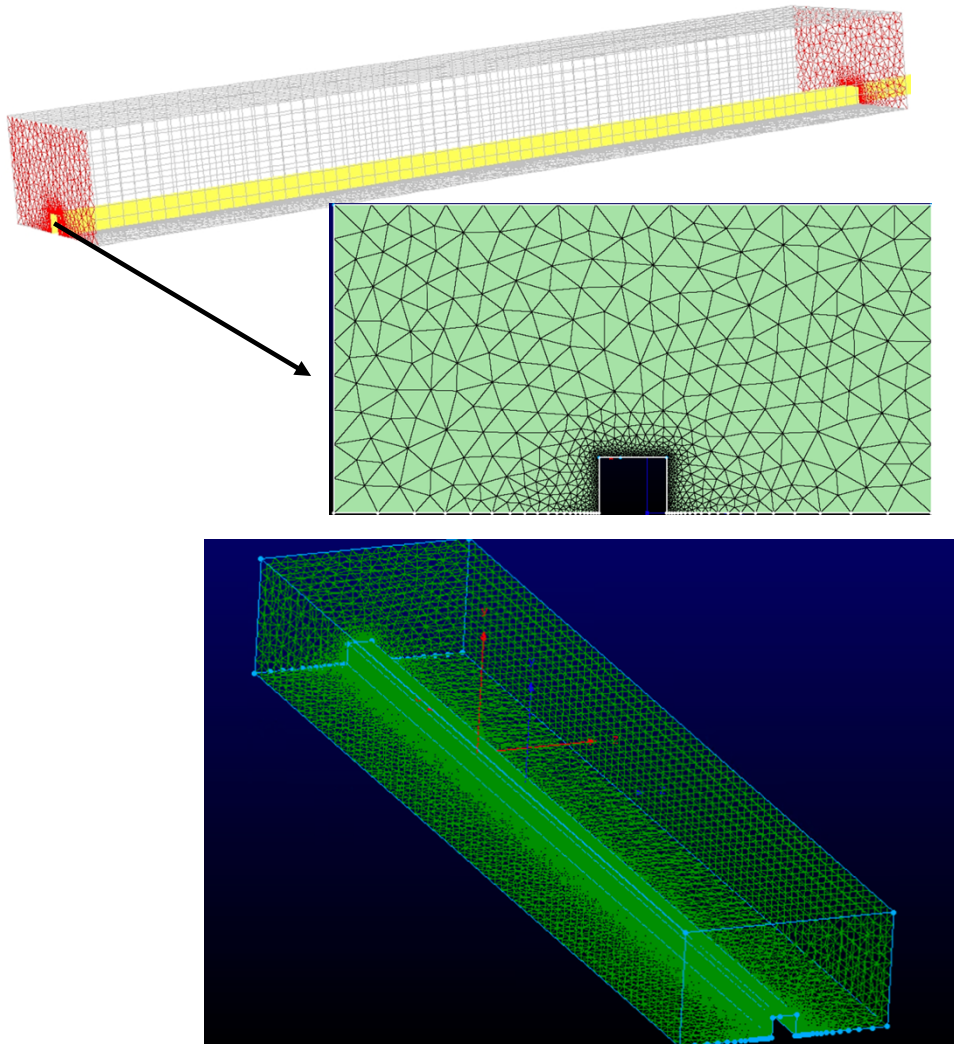
Figure 3.9 Computational domain with all dimensions.

Table 3.5 Simulation matrix

Speed	Separation Distances, ft. (m)
25 mph	2, 4, and 6 (0.61, 1.22, 1.83)
40 mph	2, 4, and 6 (0.61, 1.22, 1.83)
60 mph	2, 4, and 6 (0.61, 1.22, 1.83)

c) Dynamic Mesh and Turbulence Model

All simulations were conducted using the commercial ANSYS Fluent v.19. The smallest four-sided cell-based discretization method and temporary solver [13] were adopted in the simulations with the implementation of SIMPLE algorithm [13]. The relative speed between the truck and the cyclist was

simulated using the ANSYS Fluent sliding mesh technique. In this technique, the mesh nodes move within the dynamic mesh zone as rigid nodes. In other words, the boundaries and the mesh elements and nodes of the truck and the cyclist move rigidly within the mesh zone [14]. The deformation of the mesh in front and behind the cyclist and truck boundaries has been assigned zero deformation [14]. In addition, the mesh zone of the cyclist and the truck move relative to each other and the interface between them was linked across non-conformal boundary. The same interface was used between the mesh zone of the cyclist and the truck and the larger fluid zone enclosing them [14]. The cross non-conformal interface allows the fluid (air) to move from one mesh to another.

In addition to the dynamic mesh model, the turbulence of the fluid flow around the semi-trailer truck and the cyclist was also considered. The IDDES [12] method was used to predict the flow characteristics of the fluid engulfing the cyclist and the semitrailer truck. The IDDES method combines Delayed Detached-Eddy Simulation "DDES" [14] with an enhanced RANS-LES hybrid model [13-17]. The simulation of hybrid flows with attached and nonattached regions could be accurately performed with economical computational cost using the IDDES method. More information about the IDDES method could be found in [14].

In each simulation, side and drag forces time-history acting on the cyclist center of gravity were calculated. At each time step, cyclist side force and the truck drag were normalized by the frontal area of the cyclist, air density, and the truck relative speed. As shown in Equation 3.1:

$$Force\ Coefficient = \frac{2F}{\rho U^2 A} \tag{3.1}$$

F is the force (N), ρ is the air density (1.225 kg/m^3), u is the relative velocity magnitude of air with respect to the truck (m/s), and A is the side area of the cyclist (m^2) (0.04408 m^2)

3.3.3 Wind Tunnel Experiment

The third part of this study involved using a wind tunnel experiment to measure the side force on the cyclist using scaled 1:25 semitrailer truck and cyclist as shown in Figure 3.10. The scale of 1:25 was chosen based on the literature and to be able to provide reasonable number of elements and nodes that could be solved using the available computational tools. The aim was to compare the results with the CFD simulations and investigate the feasibility of performing scaled analysis to measure forces and how those results are compared to the field experiments. The dimensions of the truck and the cyclist were the exact same dimensions used in the CFD simulations. The cyclist and the semitrailer truck were 3-D printed as shown in Figure 3.11. All the wind tunnel experiments were conducted at the Department of Mechanical Engineering at the University of Idaho.

Figure 3.10 Scaled semitrailer truck and cyclist used in the wind tunnel simulations

The wind tunnel facility is an open circuit tunnel which has a test section of 18 in. x 18 in. (0.46 m x 0.46 m) and a length of 36 in. (.91 m), respectively. The tunnel provides variable frequencies that generates wind speed range of 1 mph (0.45 m/s) to 160 mph (71.5 m/s). In addition, the wind tunnel provides uniform air flow because it is equipped with honeycomb and wire mesh in the upstream. The test section is made of Plexiglass which can be removed from the top and bottom and is used to access and place the bicyclist and truck in the wind tunnel. The cyclist was placed on a 3-D printed mounting mechanism. The cyclist was mounted to a high-precision load cell as shown in Figure 3.11. The cyclist was positioned to the left side of the truck due to the space limitation and the test setup, however of the cyclist position was to the right, that makes no difference in the results. The whole test section was designed to minimize the vibration caused by the wind to the cyclist and the truck. On the other hand, the truck was placed on a steel plate to maintain its position and prevent it from sliding at each inflow velocity condition.
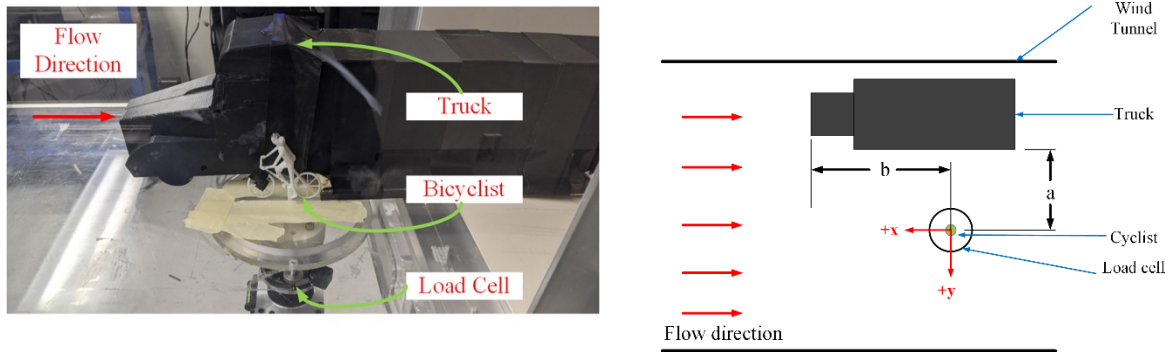
Figure 3.11 Experimental setup for bicyclist load measurements

The forces induced on the cyclist were measured in X (parallel to the wind direction), Y (perpendicular to the wind direction) and Z (vertical direction). However, for this experiment, the X and Y components were only measured. The wind tunnel is equipped with an ATI torque transducer. The transducer system was set to acquire data using a data collection rate of ~100 Hz for ~30 seconds. The prototype setting was designed to measure forces due to various cycles of steady and unsteady wind flow. The setup mechanism was designed to sense the forces directly, which were then recorded using a National Instruments (NI) data acquisition system controlled using LabView. For velocity information at each wind tunnel setting, dynamic pressure measurements were recorded using a pitot tube mounted upstream of the wind tunnel test section. The pitot tube was then attached to a manometer in which the pressure measurements were converted to velocity readings using Bernoulli's principle.

For this study, the truck position was varied in the x and y directions (i.e., a and b positions) as shown in Figure 3.11 for different wind tunnel speeds from ~5mph to ~45 mph (2.2 m/s to 20.1 m/s). At each truck position, a no wind loading scenario data was acquired to remove the bias in the load cell data. This ensures that the recorded forces were from the impact of the truck location. Table 3.6 shows the summary of the used wind speeds and the location of the cyclist relative to the truck.

Table 3.6 Test matrix showing load measurements for this investigation.
Force measurements are acquired using a 6-axis force/torque at sampling rate of ~100 Hz and sampling duration of ~100 s

Wind Tunnel Velocity, mph (m/s)	Distance from Truck (a), in. (mm)	Distance from Truck (b), in. (mm)	Force measurements
~5 (2.2)	1, 2, 3 (25.4, 50.8, 76.2)	7,10,15 (177.8, 254, 381)	✓
~12 (5.4)	1, 2, 3 (25.4, 50.8, 76.2)	7,10,15 (177.8, 254, 381)	✓

~21 (9.4)	1, 2, 3 (25.4, 50.8, 76.2)	7,10,15 (177.8, 254, 381)	✓
~26 (11.6)	1, 2, 3 (25.4, 50.8, 76.2)	7,10,15 (177.8, 254, 381)	✓
~33 (14.8)	1, 2, 3 (25.4, 50.8, 76.2)	7,10,15 (177.8, 254, 381)	✓
~40 (17.9)	1, 2, 3 (25.4, 50.8, 76.2)	7,10,15 (177.8, 254, 381)	✓
~45 (20.1)	1, 2, 3 (25.4, 50.8, 76.2)	7,10,15 (177.8, 254, 381)	✓

3.4 Results and Discussion

This section describes the results from the three methods: field tests, CFD simulations and wind tunnel experiments. The results and analysis build upon each other and therefore are described in the following subsections:

1. **Observed Wind Speeds** – Presents the measured transverse and longitudinal wind speeds under the controlled and the uncontrolled environments. In addition, a discussion on the development of the cyclist's longitudinal drag coefficient and transverse pressure coefficient have been introduced.

2. **Transverse Force and Flipping Moment Calculations** – Presents the calculations and charts that were developed for transverse wind speeds for various vehicle types, separation distances for two cyclists' profile. The results of this section have been also compared with the available literature.

3. **Longitudinal Force Calculations** – Presents the longitudinal wind forces on cyclists under the same variables used in Section 2.

4. **CFD Simulation and Wind Tunnel Results** – Presents the results, comparison, and verification with the field tests.

3.4.1 Observed Wind Speeds

The wind speeds were collected for passes of the various vehicles at a range of offset distances and vehicle speeds. Maximum speeds were limited by the need to bring the vehicle up to test speed, settle at that speed, pass through the test area, and ensure safety.

Figure 3.12 shows an example of the moving average of the transverse wind time series induced from the SUV at 25 mph (11.17 m/s) at 2 ft. (0.61 m) separation distance. As can be seen from the figure, the wind speed-time history shows pressure and suction phases at the time the vehicle passes by the

cyclist. Figure 3.12 shows three different wind speeds generated by the passing vehicle (positive, negative, and the ambient wind speed). The positive wind generates pressure that pushes the cyclists away from the passing vehicle. This pressure increases with time. The negative wind speed produces suction pressure that pulls the cyclists towards the passing vehicle and decreases with time. The difference between positive and negative is called a flip over from the positive to the negative phase. The flip over starts when the vehicle front is passing by the cyclist and its time is cited to be around 0.08 seconds. After the suction phase, the wind speeds decline to the ambient wind and at this stage, the wind pressure might have some oscillation for a few seconds. From the traffic safety point of view, the flip over phase with the instantaneous change from pressure to suction is the most interesting and relevant time interval. During the flip over time, a rapid change of the force level might produce disturbance and imbalance that might lead to the cyclist losing control and falling. In addition, the imbalance also depends on the instant reaction of the cyclist to that force level. The results of this study focuses on the flip over phase that might have an impact on the safety of cyclists or the surrounding traffic. The field tests have been conducted to measure the longitudinal and transverse wind speeds produced by overtaking vehicles. The wind speed-time history has been collected for various vehicles, speed limits and various separation distances between the cyclist and the overtaking vehicles.
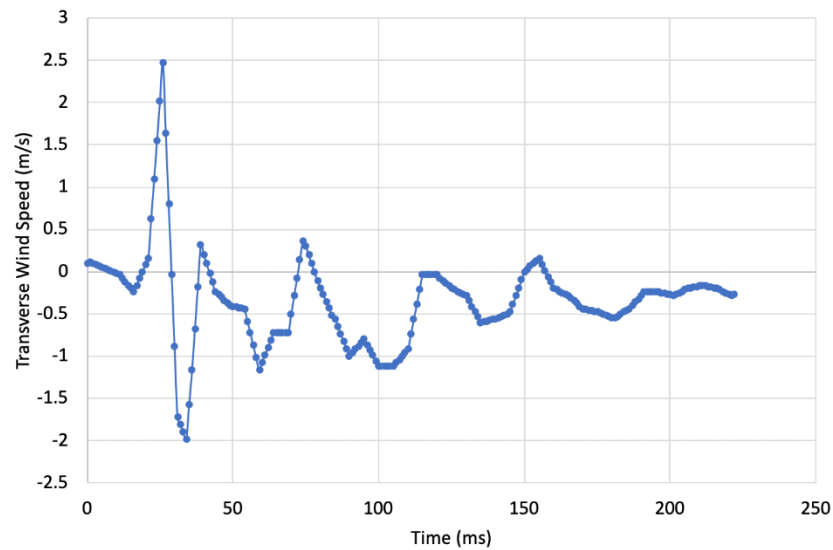

Figure 3.12 moving average of the transverse wind (SUV at 25 mph).

3.4.1.1 Controlled Environment

The controlled tests are defined as the field tests were conducted under specific circumstances to minimize the surrounding interference with the collected data. The controlled tests were performed in

Moscow, ID where traffic was minimum and to ensure that the wind speed and forces generated on cyclists are only produced by the test vehicle. In addition, the days of testing were chosen to have very close weather conditions in terms of temperature and ambient wind speeds.

The longitudinal and transverse wind speeds exerted on a cyclist were measured for four vehicle types and under three separation distances and three vehicle speeds as described in the methodology section. Each test was repeated at least five times resulting in 197 data points. Figure 3.13 shows all the data points of transverse and longitudinal wind speeds versus the separation distance for all vehicles. As can be seen, the values of the longitudinal wind speeds were higher than the transverse wind speed exerted on the cyclist and they both (longitudinally and transversally) decrease with increasing the separation distances regardless of the vehicle type. As expected, the semi-trailer truck showed the highest wind speeds in both directions, followed by the single unit truck. The pickup truck and the SUV showed very close wind speeds and that might be attributed to the fact that they have very close frontal areas.
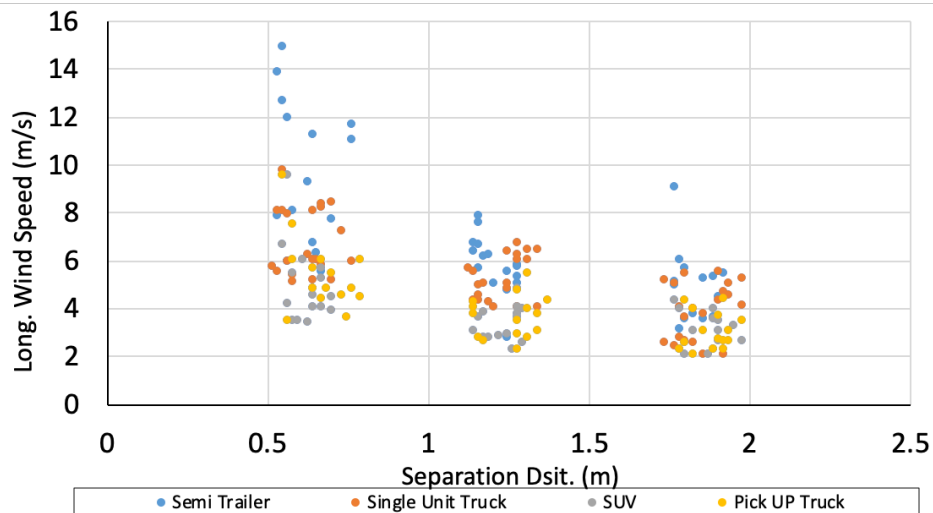
(a) Longitudinal Wind Speed vs. Separation Distance
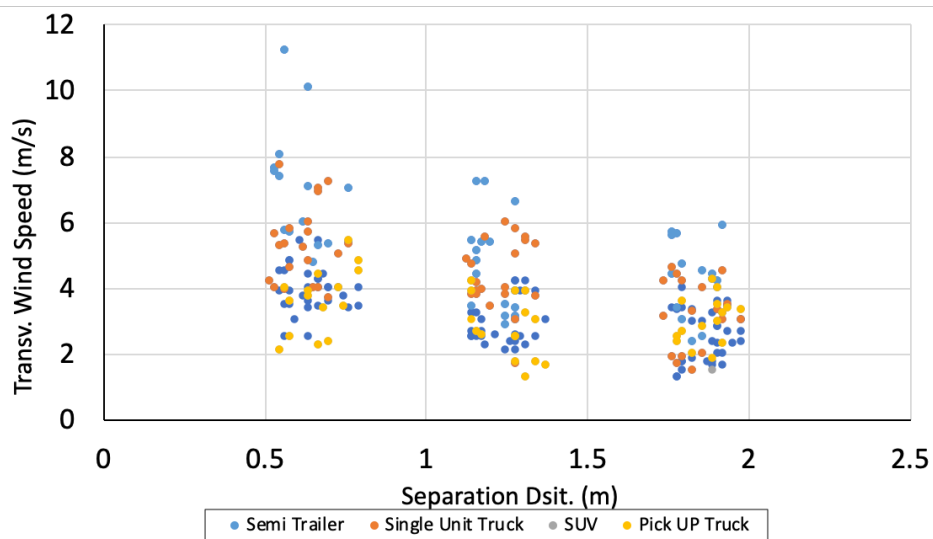
(b) Transverse Wind Speed vs. Separation Distance

Figure 3.13 All test data versus separation distance

Figure 3.14 shows the average longitudinal and transverse wind speeds versus the vehicle speed and the separation distances. The average values were calculated based on the number of repetitions of each test which was mostly five times per test. The average longitudinal and transverse wind for the semi-trailer truck speeding at 60 mph (26.82 m/s) at 2 ft. (0.61 m) were 28.82 mph (12.882 m/s) and 19.78 mph (8.845 m/s), respectively. While the SUV showed the lowest average of 14.3 mph (6.396 m/s) and 10.33 mph (4.62 m/s) at the same vehicle speed of 60 mph (26.82 m/s) at 2 ft. (0.61 m)

separation distance. The transverse wind speed is the component of wind that will be used to calculate the transverse forces on the cyclist and will be presented in the next sections.

(a) Longitudinal Wind Speed

(b) Transverse Wind Speed
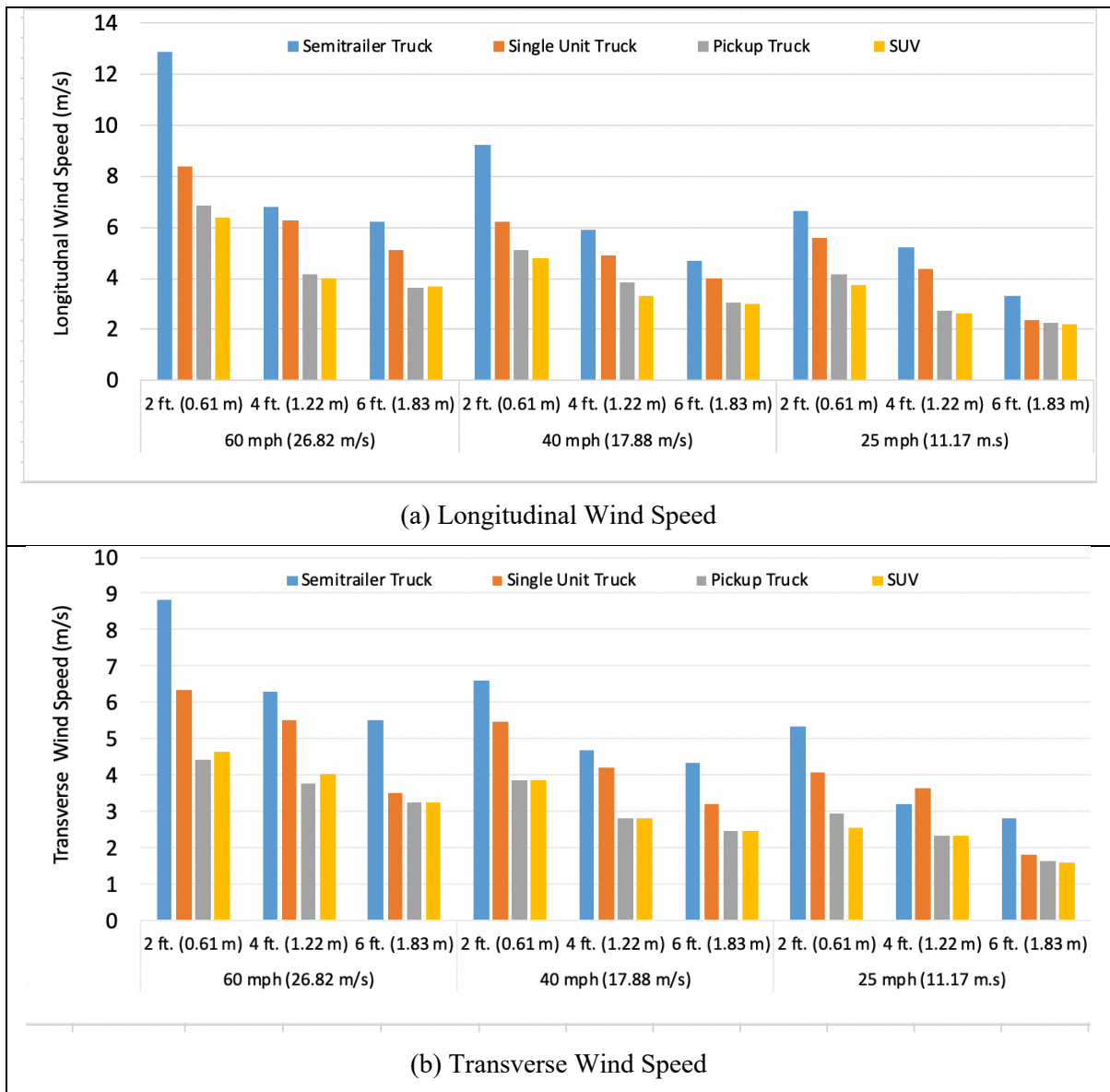
Figure 3.14 Average longitudinal and transverse wind speed
versus vehicle speeds and separation distance

A multi-regression analysis was conducted to develop a model that could be used to predict the longitudinal and transverse wind speeds based on the input data of vehicle speed, separation distance and the vehicle type. Tables 3.7 and 3.8 show the results of the regression analysis for both the longitudinal and transverse directions. The results show that the separation distance, vehicle type and vehicle speeds had significant effect ($p<0.05$) on the wind speed prediction. The separation distance

had the lowest *p* value, which meant that it had the highest effect on the longitude and transverse wind speed predictions either on the transverse or the longitudinal directions. The correlation coefficient (*r*) between the longitudinal and the transverse winds, vehicle speed, separation distance, and the vehicle type was calculated. The *r* values are shown in Tables 3.7 and 3.8 with strong relationship between all the independent factors (vehicle speed, separation distance, and vehicle type).

Table 3.7 Multi-regression results for the longitudinal wind speeds

	Coefficients	*Standard Error*	*P-value*	*r*
Intercept	7.33	0.38	0.00	N/A
Truck Speed	0.16	0.01	0.00	-0.53
Separation Distance	-2.4	0.17	0.00	-0.66
Vehicle Type	-0.94	0.08	0.00	0.56

$* R^2 = 72.4\%$

Table 3.8 Multi-regression results for the transverse wind speeds

	Coefficients	*Standard Error*	*P-value*	*r*
Intercept	5.47	0.26	0.00	N/A
Truck Speed	0.12	0.01	0.00	0.56
Separation Distance	-1.55	0.12	0.00	-0.59
Vehicle Type	-0.74	0.05	0.00	-0.60

$*R^2 = 74.3\%$

Figure 3.15 a and b show the residual plots of the controlled longitudinal and transverse wind speeds based on the developed models. The R^2 represents the variance in the wind speed (longitudinal and transverse) that is predictable from the vehicle speed, separation distance, and the vehicle type. The R^2 was 72.42% for the longitudinal direction and 74.3% for the transverse direction. In addition, the Root Mean Square Error (RMSE) was found to be 1.17 and 0.82 for the longitudinal and transverse directions.
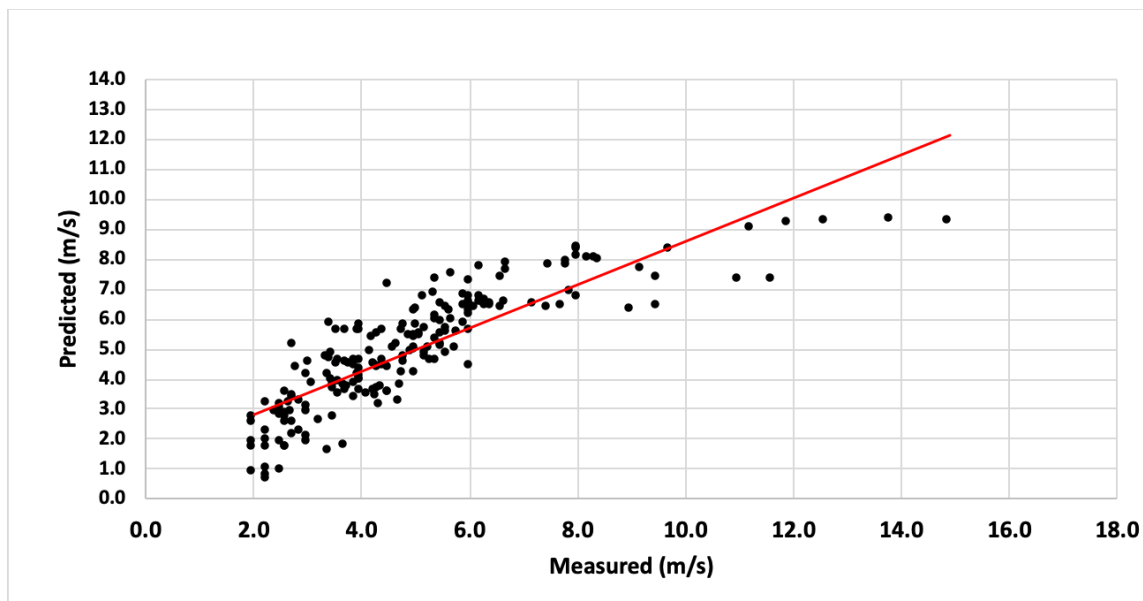
(a) Longitudinal Wind Speed, R^2=72.4%
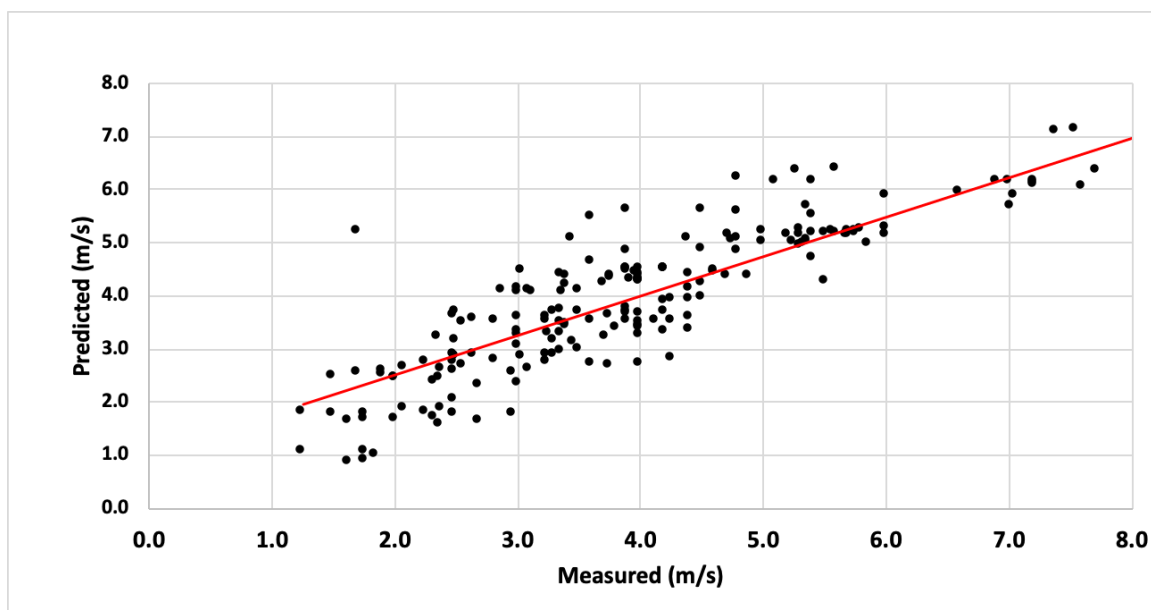
(b) Transverse Wind Speed, R^2=74.3%

Figure 3.15 Residual plots of the controlled longitudinal and transverse wind speeds

3.4.1.2 Controlled Environment

A 197 data points have been measured under the controlled test. This data was measured in the field using under various vehicle types and vehicle speeds on route US 95. The controlled data was measured in a highway section that has real/normal traffic volume, which might be the case where

cyclists use it in daily outdoor activities. Therefore, the developed models from the controlled test need to be validated under real traffic volumes and movement, which is the motivation behind the analysis conducted in this section.

Wind speed measurements have been taken from a busy highway (US 95) segments under various traffic conditions (various vehicle types and speeds). The uncontrolled test has been at multiple segments with different speed limits of 25 mph, 40 mph and 60 mph (11.17 m/s, 17.88 m/s and 26.82 m/s). The uncontrolled study has focused on the same type of vehicles and separation distances that were used under the controlled test to maintain consistency in data analysis. There was a big challenge during the controlled test, where many drivers drove away (switching lanes) from the test setup to maintain a safe distance from the wind sensor location. To overcome this problem, a real cyclist on a 26-inch bike was used with the ultrasonic wind sensor to capture the wind speed measurements. In addition, a radar speed gun was used to measure the vehicle speed because in this test vehicle speeds were not under control. A laser meter was also used to measure the actual separation distance between the cyclist and the passing vehicle.

Figure 3.16 shows the residual plots of the uncontrolled longitudinal and transverse wind for the uncontrolled case. The R^2 was 70.41% for the longitudinal direction and 71.04% for the transverse direction. In addition, the RMSE was found to be 0.75 and 0.96 for the longitudinal and transverse directions. It was noticed that the values for R^2 for the uncontrolled are less than the values obtained from the controlled case. This might be attributed to the overlap of inbound and outbound traffic during the data collection and might be due to the exiting ambient wind directions.

(a) Longitudinal Wind Speed, $R^2=70.4\%$

(b) Transverse Wind Speed, $R^2=71.04\%$
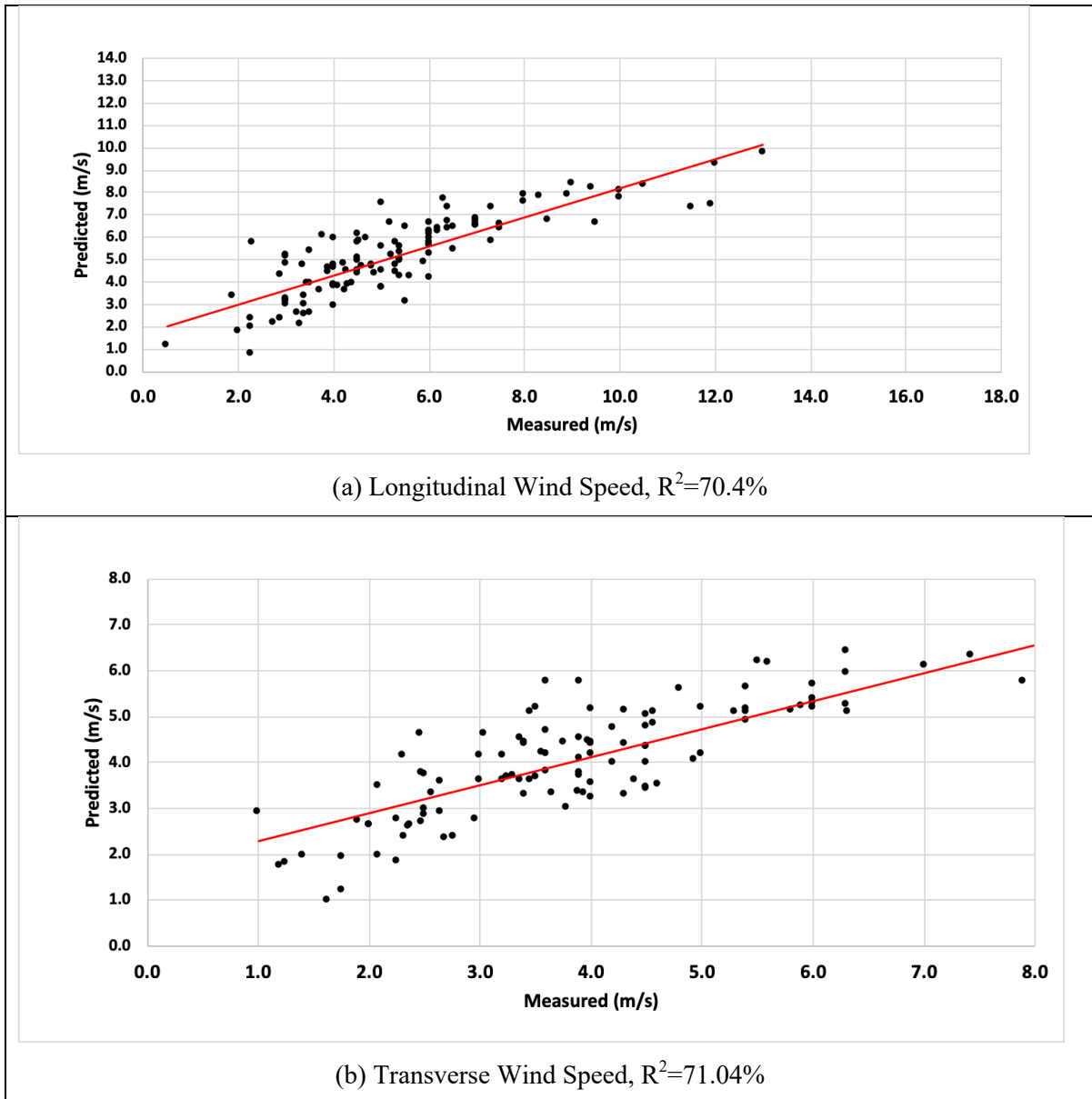
Figure 3.16 Residual plots of the uncontrolled longitudinal and transverse wind speeds

In conclusion, the developed equations from the controlled test case were validated using the uncontrolled data with a reasonable agreement in terms of the R^2 which was 70.4% and 71.04% for the longitudinal and transverse direction, respectively. Therefore, the wind speeds obtained from the controlled test were used in the following sections to calculate the transverse, longitudinal wind forces, and flipping moments as will be discussed next.

Equation 3.2 shows the general formula that was used in calculating the longitudinal forces:

$$F_L = C_D . A \frac{1}{2} \rho U^2 \qquad (3.2)$$

As can be seen, the longitudinal force, F_L depends on the cyclist frontal area (A), air density (ρ), and the longitudinal wind speed (U). In this study, the magnitude of the difference between the first positive peak and negative peak of wind speeds were calculated based on the measured wind-time-history, and C_D is the drag coefficient which depends on the cyclist position (upright or racing position).

Equation 3.2 could also be used to calculate the transverse force, F_T, on a cyclist. However, the only difference is the coefficient C_D that was replaced by another transverse force/pressure coefficient, C_P (will be discussed next) that depends on the vehicle type, vehicle speed and the separation distance between the cyclist and the vehicle. The drag coefficient C_D is a very well-known number that has been experimentally measured for various bikes and cyclists and could be found in the literature [5]. The C_D coefficient represents the resistance of the cyclist's geometry and shape to the flowing air facing the cyclist and parallel to the movement direction.

The challenge exists when it comes to calculating the transverse force (perpendicular to traffic direction), where there is no data available about transverse force/pressure coefficient C_P. This coefficient was calculated from the field tests for every vehicle type and depended on separation distance between the cyclist and the passing vehicle.

To obtain the C_p coefficient, the observed/measured longitudinal and transverse wind speeds have been normalized (divided by vehicle speed), U/U_v and plotted against the observed separation distances measured from the field test. The U/U_v equals the C_p factor, based on the work cited from [6]. The relationship between the normalized wind speeds and the separation distances were represented by a power function. Figure 3.17 shows the procedure used to calculate the transverse and longitudinal forces on cyclists.
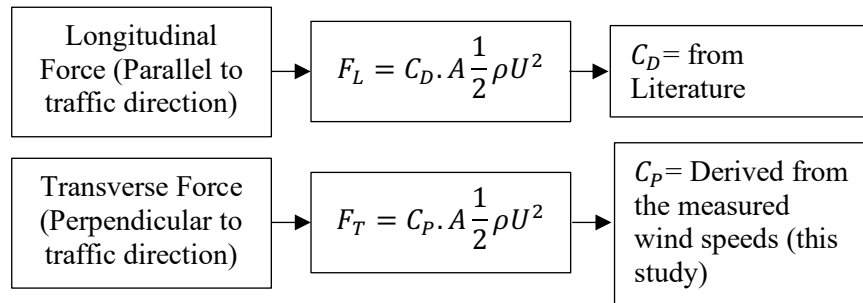
Figure 3.17 procedure used to calculate the transverse and longitudinal forces

Figure 3.18 shows normalized transverse wind speed versus the separation distance for the four vehicles tested. The relationship between the normalized wind speed (U/U_v) and separation distance was correlated using power functions. Figure 3.18 shows all the developed power functions with the corresponding R^2 for each tested vehicle. The separation distances were varied from the designed ones due to the difficulty of the driver to center the front tire of the vehicle over the pavement marker at 2, 4 and 6 ft. (0.61, 1.22, and 1.83 m) from the wind sensor location.

Table 3.9 summarized all the developed power functions and the corresponding coefficient of determination, R^2. It can be seen that all the R^2 is in the range of 43.82% to 55.96%.

Table 3.9 Normalized wind speed for tested vehicles (U/U_v), the C_p Coefficient

	Transverse Direction	R^2
Semitrailer Truck	$0.2971x^{-0.458}$	55.96%
Truck	$0.2407x^{-0.465}$	50.27%
Pickup Tuck	$0.1773x^{-0.407}$	43.82%
SUV	$0.1719x^{-0.353}$	50.35%
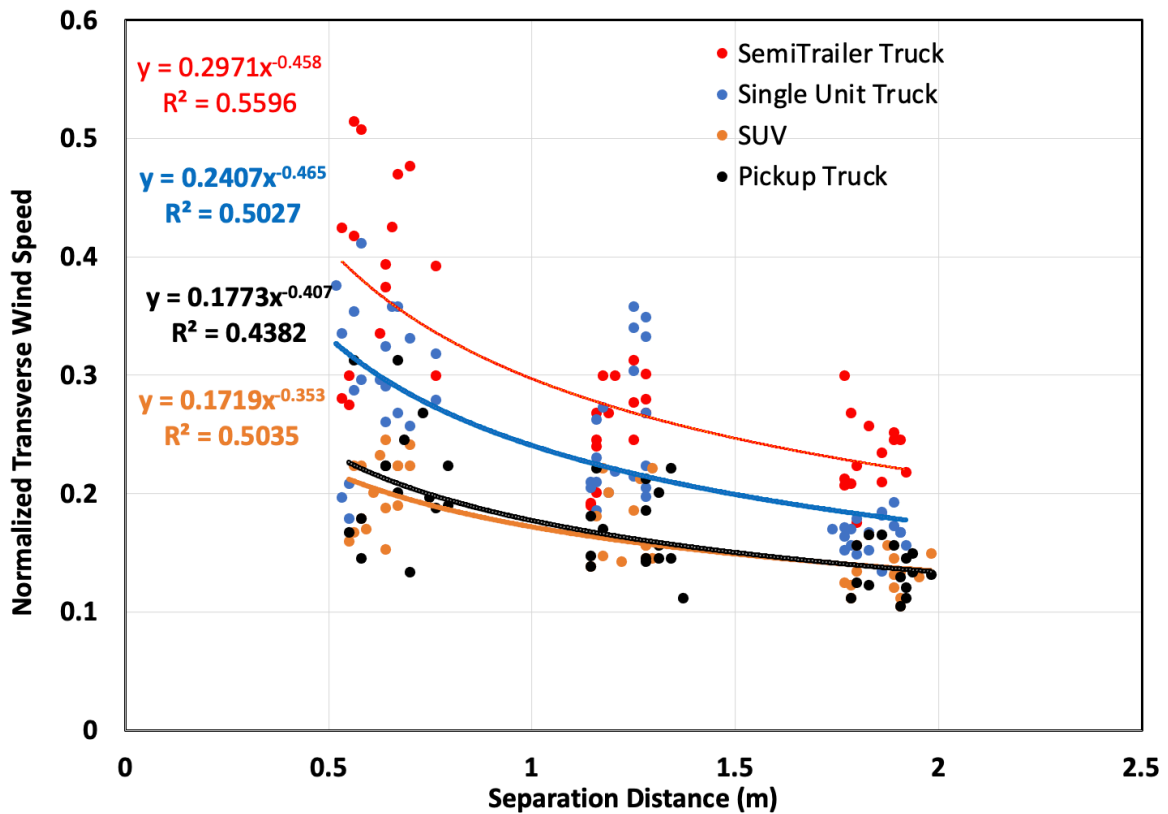
Figure 3.18. Normalized transverse wind speed vs. the separation distance for all cases

The measured normalized transverse wind speed has been compared to the exiting data in the literature for verification purpose. Lubitz et al. (2018) [7] has measured the normalized transverse wind speed using only one vehicle, which was the same pickup truck that was used in this study (Dodge Ram). Figure 3.19 shows the comparison of the normalized transverse wind speed versus the separation distance. Figure 3.19 shows that the results are in agreement when they compared for separation distances larger than 2 ft. (0.61m). The threshold of 2 ft. (0.61m) is representative because vehicles closer than 2 ft. is not logical because it threatens cyclist safety. The percent of difference between this study and [7] was 31.7% at 2 ft. (0.61 m) and 5.9% at 4 ft. (1.22 m). The other U/U_v for other vehicles in this study (SUV, single unit truck, and semi-trailer truck) versus the separation distances are shown in Figure 3.19. The Figure shows that the U/U_v values are highest for the semitrailer and lowest for the SUV and the pickup truck. The U/U_v factor will be used in the force calculations where it accounts for the separation distances, vehicle type and the transverse wind speed generated by the overtaking vehicle.
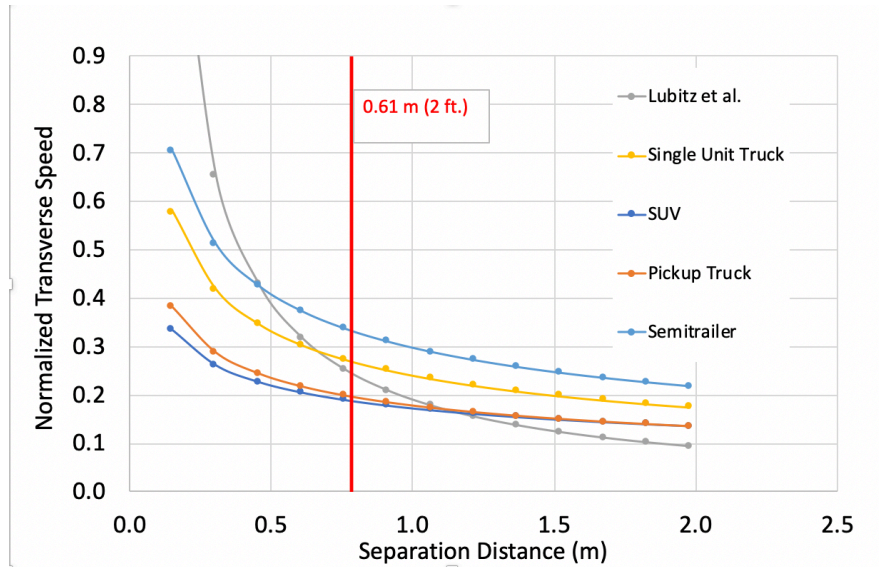
Figure 3.19 Comparison between Lubitz et al. and the results of this study.

3.4.2 Transverse Force and Flipping Moment Calculations

Cyclist experience two types of forces when they are overtaken by passing vehicles. The longitudinal and transverse forces could be calculated from multiplying the longitudinal and transverse pressures by the frontal and side areas of the cyclist, respectively. Equation 3.2 has been rearranged to represent pressure instead of force.

The longitudinal pressure (P_L) which is parallel to the direction of vehicle movement depends on the cyclist drag coefficient (C_D), air density (ρ), and the longitudinal wind speed (U_L). Equation 3.3 was used to calculate the longitudinal pressure on a cyclist. This pressure is a sudden (instantaneous) pressure that hits the cyclist in a very short period of time, usually in milliseconds. The longitudinal force was calculated from Equation 3.4, by multiplying the pressure by the frontal area of the cyclist.

$$P_L = \frac{C_D \rho U_L{}^2}{2} \tag{3.3}$$

$$F_L = P_L A_F \tag{3.4}$$

Where, the cyclist frontal area (A_F).

The second aerodynamic pressure, P_T represents the transverse wind pressure induced on the cyclist. This pressure depends on air density (ρ), side area (A_S), transverse wind speeds (U_T), and the

coefficient Cp. The factor Cp is dimensionless and represents the streamlining of wind flow and depends on the vehicle speed, the transverse wind speed and the separation distance between the cyclist and the vehicle (please see normalized wind speed analysis) section as seen in Equation 3.4.

$$P_T = \frac{C_p \rho U_T{}^2}{2} \tag{3.5}$$

Similarly, the transverse force was calculated from Equation 3.5, by multiplying the transverse pressure by the side (transverse) area of the cyclist.

$$F_T = P_T A_S \tag{3.5}$$

Where, the cyclist frontal area (A_S).

There are two surface areas for a cyclist, the frontal area and the side/transverse area. The side area was the area used to calculate the transverse forces, while the frontal area was the area is the one used to calculate the longitudinal forces (perpendicular to the vehicle movement direction) on a cyclist. Table 3.10 summarized all the frontal and side areas and the drag and Cp coefficients used in this study.

Table 3.10 Cyclist's parameters used in this study

	Frontal area	**Side Area (A_s)**	**C_p**	**C_D [5]**
Cyclist	0.55 m² [5]	8.5 ft² (0.79 m²)	Table 3.9 C_p is function of the separation distance	0.9 Racing
		10.11 ft² (0.94 m²)		1.1 Upright commuter
		12.27 ft² (1.14 m²)		

The information listed in Table 3.10 was used to calculate the longitudinal and transverse forces on the cyclists. The forces were calculated for the four (4) types of vehicles under the effect of all the parameters shown in Table 3.10 as will be discussed below. The forces have been used to calculate the flipping moment by using Equation 3.6 with a moment arm (L) of 0.87 [6].

The flipping moment was calculated based on simple mechanics as shown in Equation 3.6:

$$M = F_T . L \qquad\qquad (3.6)$$

Where M is the flipping moment, F_T is the transverse force and L is the experimental moment arm.

The FHWA, 1977 [10] criteria digest described the aerodynamic impact of vehicles on cyclists as "Aside from the noise impact caused by heavy vehicles, a direct safety concern is the effect of the aerodynamic force from those vehicles place on the cyclist. At certain speeds a truck can create enough aerodynamic force to spill a cyclist. When vehicle speeds exceed the "tolerance limit" a separation should be provided. If the force cannot be reduced, another bikeway location should be studied regardless of the trucking activity" [10] .

The flowing section presents flipping moments for various vehicles, vehicle speeds, separation distances and cyclists. Figures 3.20-3.22 show the flipping moment charts for all vehicles corresponding to a cyclist side area of 8.5 ft^2 (0.79 m^2), 10.11 ft^2 (0.94 m^2), and 12.27 ft^2 (1.14 m^2), [5]. All the moment values have been compared to the FHWA 1977 tolerance limit, which is 15 N.m [FHWA 1977, 10].

- Cyclist with side area of 8.5 ft^2 (0.79 m^2)

The flipping moment (FM) is defined as the transverse force (perpendicular to the cyclist movement direction) multiplied by the moment arm (distance between the c.g. of the cyclist and the ground surface). As can be seen in Figure 3.20, the largest flipping moment was produced by the case of the semi-trailer truck and then decreased with the single unit truck. The SUV and the pickup truck showed close flipping moment values. The highest flipping moment was 88.79 lb. ft. (120.38 N.m) when the semi-trailer truck had a speed of 60 mph (26.82 m/s) and 2 ft (0.62 m) separation distance and that value was high above the tolerance limit of 11.06 lb.ft. (15 N.m) [9]. The FM was below the tolerance limit for the semi-trailer truck at a speed of 25 mph (26.82 m/s) and separation distance of 3.61 ft. (1.1 m). However, the FM of the semitrailer truck was above the tolerance limit for all other cases of separation distances and the vehicle speeds.

The FMs were lower for the case of a single unit truck compared to the semi-trailer truck as shown in Figure 3.20. The highest FM was 37.28 lb.ft. (50.55 N.m) at speed 60 mph (26.82 m/s) and 2 ft (0.62 m) separation distance. The FMs went below the tolerance limit at separation distance of 2.62 ft. (0.8 m) that is corresponding to vehicle speed of 25 mph (11.17 m/s). In addition, the FM had an inflection point at a separation distance of 4.10 ft. (1.25 m) at vehicle speed of 40 mph (17.88 m/s). On the other hand, the SUV and the pickup truck showed lower FM values compared to the tolerance limit [9], except the case of a SUV speeding at 60 mph (26.82 m/s) and separation distance of 3.28 ft. (1.0 m).
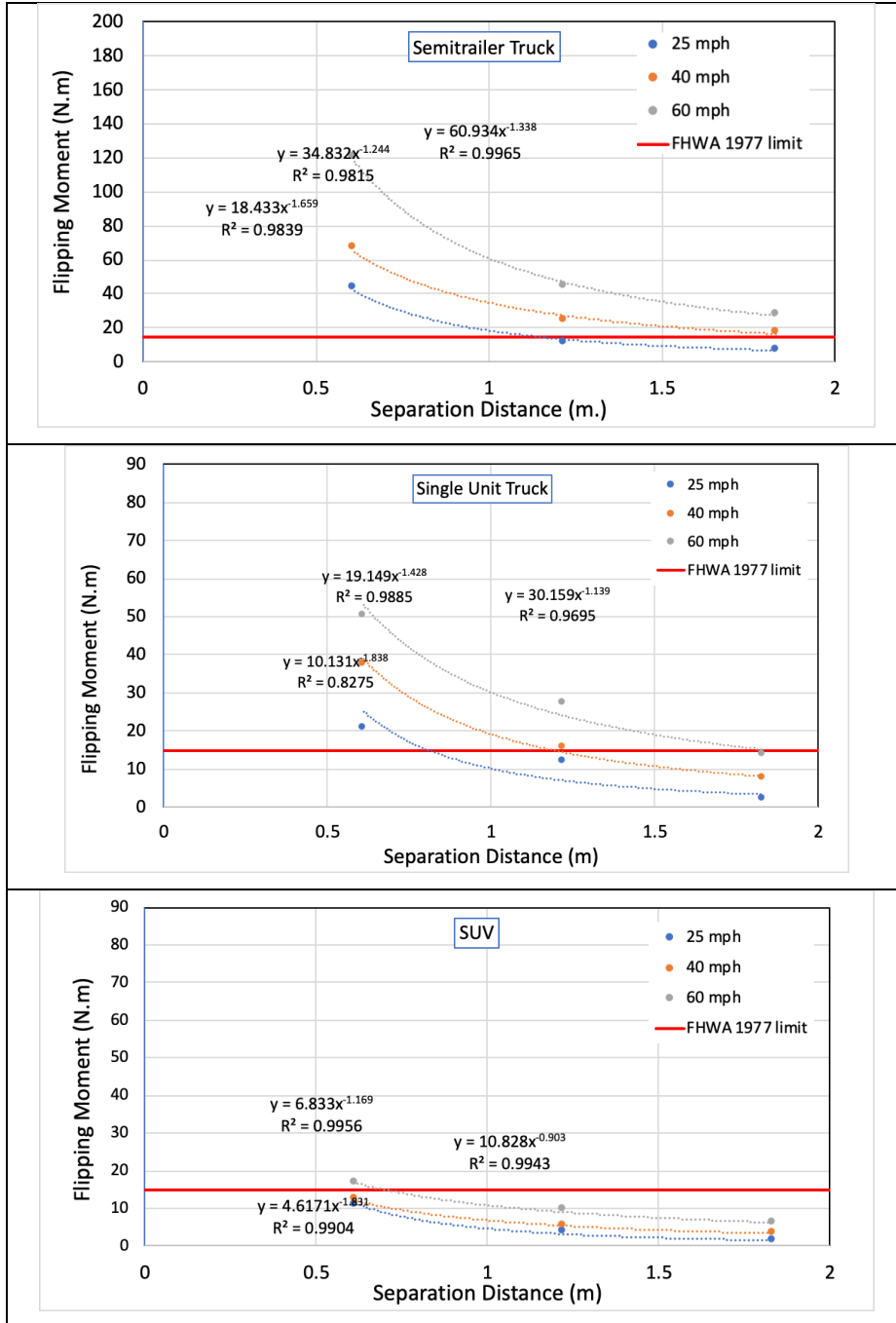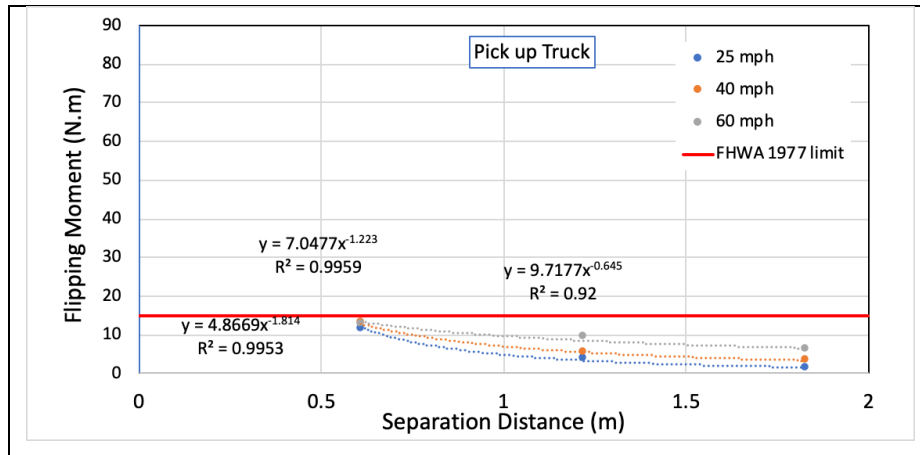
Figure 3.20 Force and moments on cyclist with side Area of 8.5 ft² (0.79 m²)

- Cyclist with side area of 10.11 ft² (0.94 m²)

As can be seen in Figure 3.21, the flipping moment followed the same trend in the previous cyclist cross sectional area. The highest flipping moment was 105.64 lb. ft. (143.23 N.m) when the semi-trailer truck had a speed of 60 mph (26.82 m/s) and 2 ft (0.62 m) separation distance and that value exceeded the tolerance limit of 11.06 lb.ft. (15 N.m) [10]. For the semi-trailer truck at a speed of 25 mph (26.82 m/s), the FM was above the tolerance limit at smaller separation distances, then at a separation distance of 4.1 ft. (1.25 m)., It went below the tolerance limit. However, the FM of the semi-trailer truck was above the tolerance limit for all other cases of the various separation distances and the vehicle speeds.

For the single unit truck, the FMs were smaller compared to the semitrailer truck. The highest FM was 44.36 lb.ft. (53.81 N.m) at a speed of 60 mph (26.82 m/s) and 2 ft (0.62 m) separation distance. The FMs went below the tolerance limit at separation distance of 2.9 ft. (0.9 m) at a vehicle speed of 25 mph (11.17 m/s). In addition, the FM had an inflection point at a separation distance of 2.78 ft. (0. 85 m) at vehicle speed of 40 mph (17.88 m/s). It can be seen that there was a significant drop of 58% in the FM between the semi-trailer and the single unit truck for a vehicle speed of 60 mph (26.82 m/s) and 2 ft (0.62 m). On the other hand, the SUV and the pickup truck showed lower FM values compared to the FHWA limit, except the case of a SUV speeding at 60 mph (26.82 m/s) and separation distance of 2.46 ft. (0.75 m).
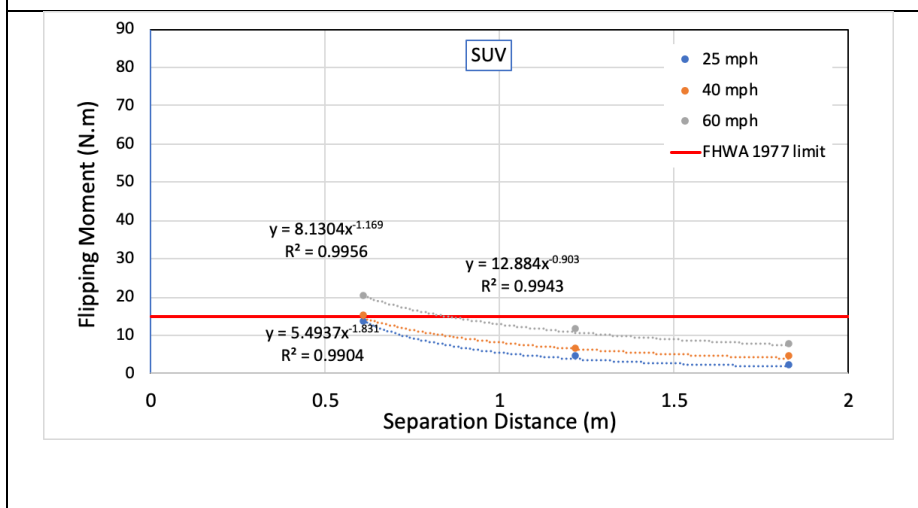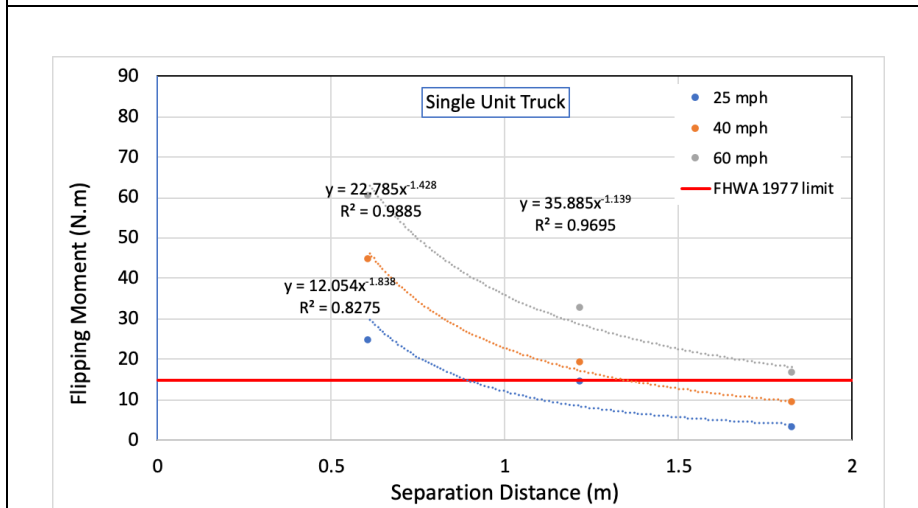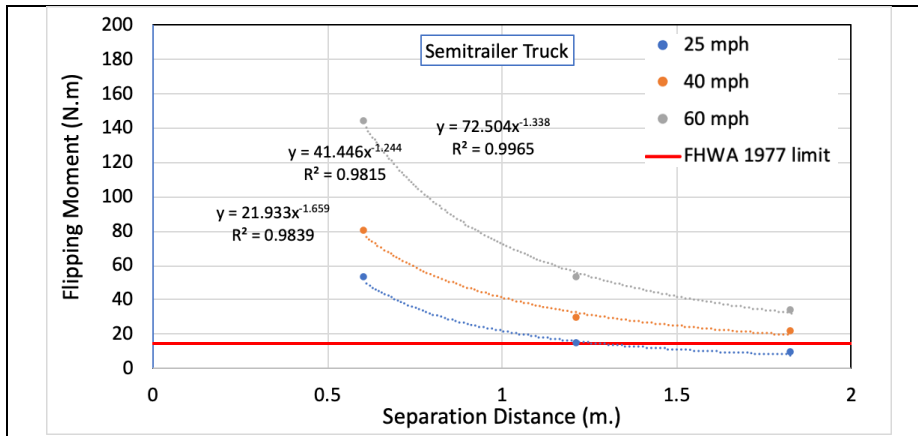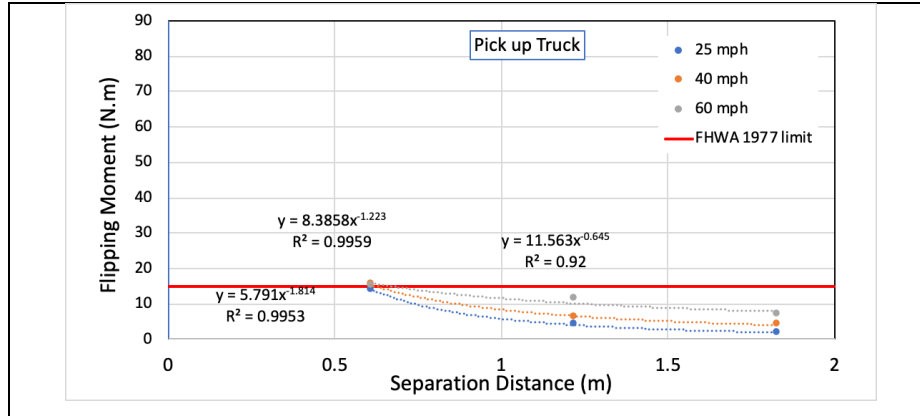
Figure 3.21 Force and moments on cyclist with side Area of 10.11 ft² (0.94 m²)

- Cyclist with side area of 12.27 ft² (1.14 m²)

As can be seen in Figure 3.22, The SUV and the pickup truck showed close FM values. The highest FM was 128 lb. ft. (173.71 N.m) when the semi-trailer truck had a speed of 60 mph (26.82 m/s) and 2 ft (0.62 m) separation distance and that value exceeded the tolerance limit of 11.06 lb.ft. (15 N.m). The FM was below the tolerance limit for the semitrailer truck at a speed of 25 mph (26.82 m/s) and separation distance of 4.9 ft. (1.5 m). However, the FM of the semi-trailer truck was above the tolerance limit for all other cases of the separation distances and the vehicle speeds.

The FMs were lower for the case of single of unit truck compared to the semi-trailer truck. The highest FM was 72.95 lb.ft. (53.81 N.m) at speed 60 mph (26.82 m/s) and 2 ft (0.62 m) separation distance. The FMs went below the tolerance limit at separation distance of 2.9 ft. (0.9 m). In addition, the FM had an inflection point at a separation distance of 4.92 ft. (1.5 m) at vehicle speed of 40 mph (17.88 m/s). It can be seen that there was a significant drop of 58% in the FM between the semitrailer and the single unit truck for a vehicle speed of 60 mph (26.82 m/s) and 2 ft (0.62 m). On the other hand, the SUV and the pickup truck showed lower FM values compared to the tolerance limit, except the case of a SUV speeding at 60 mph (26.82 m/s) and separation distance of 3.28 ft. (1.0 m).

Semitrailer Truck

y = 87.931x^{-1.338}
R² = 0.9965

y = 50.264x^{-1.244}
R² = 0.9815

y = 26.6x^{-1.659}
R² = 0.9839

• 25 mph
• 40 mph
• 60 mph
— FHWA 1977 limit

Single Unit Truck

y = 27.633x^{-1.428}
R² = 0.9885

y = 43.52x^{-1.139}
R² = 0.9695

y = 14.619x^{-1.838}
R² = 0.8275

• 25 mph
• 40 mph
• 60 mph
— FHWA 1977 limit

SUV

y = 9.8603x^{-1.169}
R² = 0.9956

y = 15.626x^{-0.903}
R² = 0.9943

y = 6.6626x^{-1.831}
R² = 0.9904

• 25 mph
• 40 mph
• 60 mph
— FHWA 1977 limit
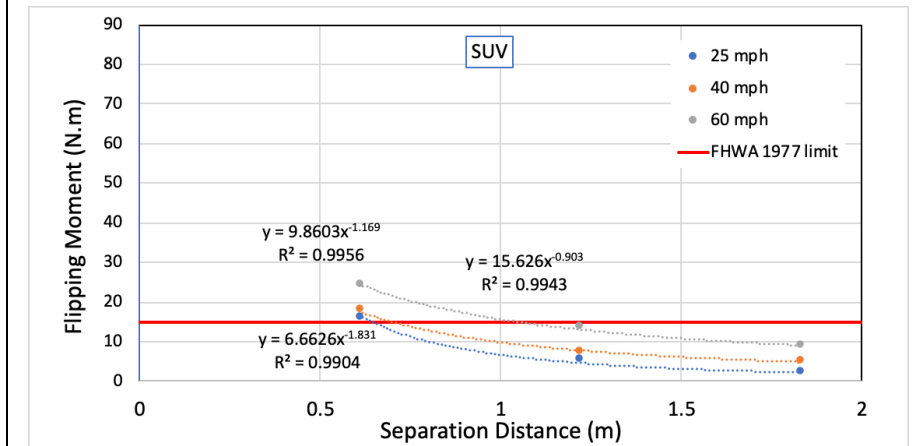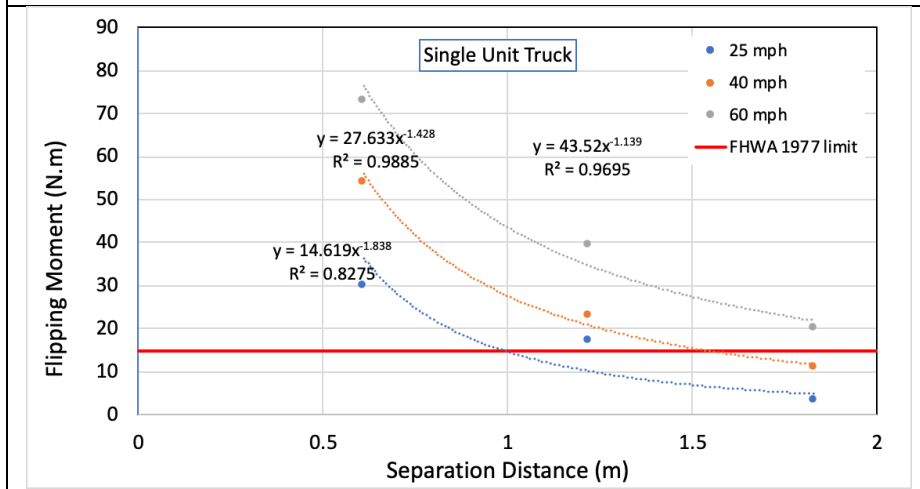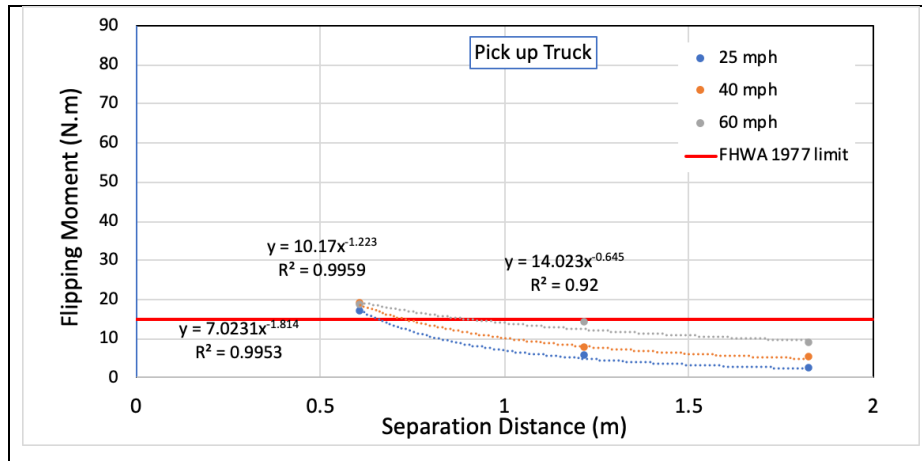
Figure 3.22 Force and moments on cyclist with side Area of 12.27 ft^2 (1.14 m^2)

The results of the present study have been compared with all the available data in the literature. Table 3.11 shows a summary of the available transverse forces on cyclists resulting from passing vehicles. It can be seen from Table 3.11 that there are differences between induced forces on cyclists under same testing conditions and this is attributed to the huge variation of vehicle muzzle shapes and frontal areas and side area of the vehicles. For example, Lee 2009 [11] has studied the induced forces on cylindrical dummy shape (simulation of a human body) by a passing high-speed train. The train had a steep tapered nose, and the transverse force measures were found to be 15.51 lb. (69 N) at a speed of 148 mph (66.38 m/s), which is smaller than the force induced in this study by a semitrailer truck at a speed of 60 mph (26.82 m/s)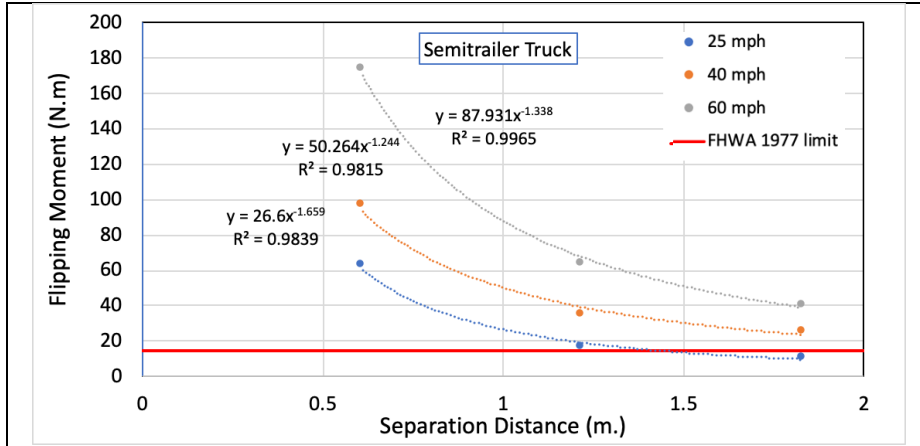 at a separation distance of 2.00 ft. (0.61m/s). If the train has a bluff nose that might be compared to the frontal area of truck, the transverse force was reported to be 28.1 lb. (125 N) at a speed of 114 mph (51.1 m/s). Lee 2009 [11] and other has reported that aerodynamics and the frontal area of the vehicle has a significant effect on the aerodynamic forces induced on cyclists.

In addition, it is noticed in Table 3.11 that semitrailer trucks that have been used in various studies have different aerodynamic characteristics, which induce different forces. The calculated transverse forces measured in this research are close to the values reported by Lichtneger et al. [5] (Forces on roadside plates) as shown in Table 3.11. However, there are discrepancies between all the published articles.

Table 3.11 Comparison of results

Study	Vehicle Speed, mph (m/s)	Side Area, ft² (m²)	Separation Dist. ft., (m)	Vehicle Type	Force, lb. (N)
Lichtneger et al. [5]	45 (20.11)	24.2 (2.25)	1.6 (0.49)	Trailer Truck	38.2 (170)
	49.7 (22.2)	10.67 (1.0)			7.3 (32.5)
	45 (20.11)	2.69 (0.25)			105.6 (470)
Lubitz et al. [7]	33 (14.75)	N/A	4.43 (1.35)	Pickup Truck	1.12 (5)
Walton et al. [8]	49.7 (22.2)	5.92 (0.55)	5.0 (1.52)	Semitrailer Truck	22.4 (100)
Gromke et al. [6]	60 (26.82)	12.27 (1.14)	1.64 (0.5)	Sedan Wagon	11.6 (52)
Lee (2009) [11]	148.5 (66.38)	N/A	3.94 (1.2)	High Speed Train	15.51 (69)
This Study	60 (26.82)	12.27 (1.14)	2.00 (0.61)	Semitrailer Truck	44.73 (199)
	60 (26.82)			Single Unit Truck	18.85 (83.85)
	60 (26.82)			Pickup Truck	5.0 (21.22)

3.4.3 Longitudinal Force Calculations

In addition to the transverse forces outlined in the previous section, the longitudinal wind forces induced on cyclists were calculated and compared. Tables 3.12 and 3.13 show the values of the longitudinal forces based on all the parameters studied. In addition to the vehicle speed, separation distance and the vehicle type, the drag coefficient of the cyclist mainly affect those levels of forces. The position of the cyclist on the bike affects the drag coefficient and therefore affect the level of force induced on the cyclist. Two very common positions of bikers; upright commuter and the racing positions were equivalent to drag coefficients of 0.9 and 1.1, respectively [5] as shown in Tables 3.12 and 3.13.

Table 3.12 Longitudinal forces of Cyclist Drag Coefficient of 0.9

Vehicle Speed, mph (m/s)	Separation Distance, ft. (m)	C_D 0.9	Semitrailer Truck		Single Unit Truck		SUV		Pickup Truck	
			Long. Speed (m/s)	Long. Force (N)	Long. Speed (m/s)	Long. Force (N)	Long. Speed (m/s)	Long. Force (N)	Long. Speed (m/s)	Long. Force (N)
25 (11.17)	2 (0.61)		6.67	122.66	5.58	85.84	3.76	38.99	4.14	47.14
40 (17.88)	2 (0.61)		9.26	236.53	6.24	107.45	5.00	68.93	5.12	72.27
60 (26.82)	2 (0.61)		12.88	457.52	8.38	193.48	6.40	112.79	6.86	129.90

Vehicle Speed	Separation Distance	Semitrailer Speed	Semitrailer Force	Single Unit Speed	Single Unit Force	SUV Speed	SUV Force	Pickup Speed	Pickup Force
25 (11.17)	4 (1.22)	5.24	75.56	4.37	52.55	2.63	19.00	2.73	20.47
40 (17.88)	4 (1.22)	5.92	96.62	4.92	66.65	3.33	30.54	3.86	40.99
60 (26.82)	4 (1.22)	6.78	126.74	6.28	108.83	4.00	44.11	4.14	47.35
25 (11.17)	6 (1.83)	3.32	30.39	2.39	15.69	2.20	13.34	2.25	13.96
40 (17.88)	6 (1.83)	4.68	60.39	4.01	44.43	2.98	24.55	3.06	25.75
60 (26.82)	6 (1.83)	6.22	106.53	5.11	72.11	3.71	37.91	3.63	36.29

Table 3.13 Longitudinal forces with Cyclist Drag Coefficient of 1.1

Vehicle Speed, mph (m/s)	Separation Distance, ft. (m)	C_D	Semitrailer Truck		Single Unit Truck		SUV		Pickup Truck	
			Long. Speed (m/s)	Long. Force (N)	Long. Speed (m/s)	Long. Force (N)	Long. Speed (m/s)	Long. Force (N)	Long. Speed (m/s)	Long. Force (N)
25 (11.17)	2 (0.61)		6.67	149.91	5.58	104.92	3.76	47.65	4.14	57.62
40 (17.88)	2 (0.61)		9.26	289.09	6.24	131.33	5.00	84.24	5.12	88.33
60 (26.82)	2 (0.61)		12.88	559.19	8.38	236.47	6.40	137.85	6.86	158.76
		1.1								
25 (11.17)	4 (1.22)		5.24	92.35	4.37	64.22	2.63	23.22	2.73	25.02
40 (17.88)	4 (1.22)		5.92	118.10	4.92	81.46	3.33	37.32	3.86	50.10
60 (26.82)	4 (1.22)		6.78	154.90	6.28	133.02	4.00	53.91	4.14	57.87
25 (11.17)	6 (1.83)		3.32	37.14	2.39	19.18	2.20	16.31	2.25	17.06
40 (17.88)	6 (1.83)		4.68	73.80	4.01	54.30	2.98	30.00	3.06	31.47
60 (26.82)	6 (1.83)		6.22	130.20	5.11	88.14	3.71	46.33	3.63	44.35

It can be seen from Table 3.12 that the wind forces generated by the semi-trailer truck were way higher than other vehicles especially at drag coefficient of 1.1. The longitudinal force induced by the semi-trailer truck was higher than the single unit truck by 136.5% at a speed of 60 mph (26.82 m/s) at a separation distance of 2 ft. (0.61 m) and dropped to 47.7% at a speed of 60 mph at a separation distance of 6 ft. (1.82 m). It can be seen that the separation distance has a great influence on the longitudinal force value. The force generated from the semi-trailer at 60 mph (26.82 m/s) at separation distances of 2 ft. (0.61 m), and 6 ft. (1.82 m) were 457 N and 106 N, respectively for a drag coefficient of 1.1. Overall, the longitudinal force decreases with decreasing the vehicle speed and increases with decreasing the separation distance. Those forces are an instantaneous force and are applied as an impact forces to the cyclists in a very short period of times (0.10-0.25 seconds). No well-defined data is available in the literature to compare with the results of this study.

The forces generated by the SUV and the pickup truck were very close for both values of the drag coefficients of 0.9 and 1.1, and that was due to the same frontal area of the SUV and the pickup truck. At a speed of 60 mph (26.82 m/s) and separation distances of 2 ft. (0.61 m), the longitudinal forces were 112.8 N (25 lb.) and 129.9 (29.2 lb.) for the SUV and the pickup truck, respectively for drag coefficient of 0.9. While at a drag coefficient of 1.1, the longitudinal forces were 137.85 N (31 lb.) and 158.76 (35.7 lb.) for the SUV and the pickup truck, respectively.

Changing the drag coefficient (biker position) has a great influence on the generated force levels. As can be seen in Figure 3.23, the semitrailer truck has the highest force generated for both C_D of 0.9 and 1.1. However, the force induced by the semi-trailer truck has decreased by 22.2% for a speed of 60 mph (26.82 m/s) and separation distances of 2 ft. (0.61 m), when the drag has decreased from 1.1 to 0.9. While at a separation distance of 4 ft. (1.21 m), and 6 ft. (1.81 m), the differences between the forces were not significant for both values of the drag coeffects.
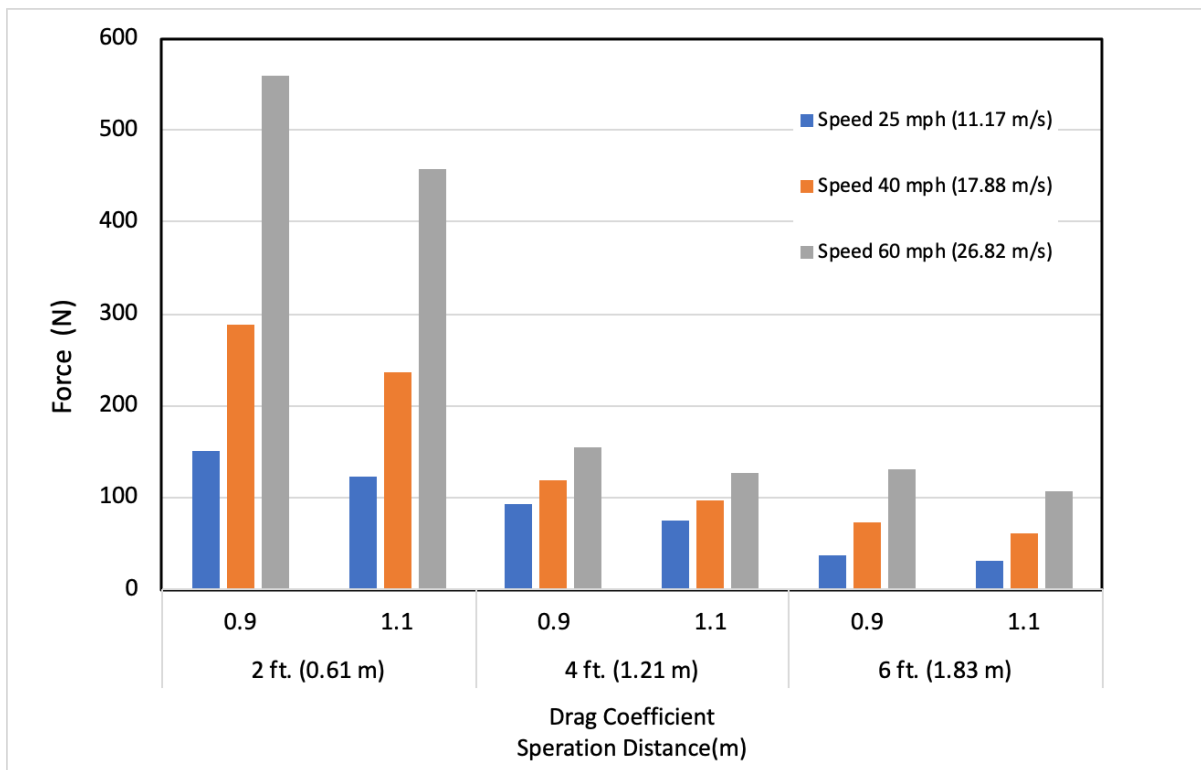

Figure 3.23 Variation of Longitudinal Wind Forces
vs. separation distances and drag coefficients.

3.4.4 CFD Modeling and Wind Tunnel Verification

This section presents the results of the CFD and the wind tunnel scaled experiments. A full description of the CFD and the wind tunnel could be found at the beginning of this chapter. The CFD models were designed to have a 1:25 scale to decrease the time of the computational effort without affecting the accuracy. A combination of nine models (cyclist and semitrailer truck) were developed under various truck speeds (25, 40, and 60 mph) and three separation distances of 2 ft., 4 ft. and 6 ft. (0.61 m, 1.22 m, 1.81 m). To minimize the computational time, the side force on the cyclist was the only output that has been chosen from the CFD.

The cyclist and the semi-trailer truck were 3-D printed to the same scale (1:25) and used in the CFD. The printed prototypes were placed in a wind tunnel to simulate the aerodynamic characteristics of a typical cyclist under a passing truck. It could not be possible to fix cyclist in position and move the truck with various speeds. Instead, the truck and the cyclist were fixed in place inside the wind tunnel and various wind pressures were applied to both of them. The wind pressure was designed to generate almost the same wind speed of the moving semi-trailer truck in the CFD simulations. Table 3.4 shows all the tested cases.

Figure 3.24 shows a typical transverse force time history for a cyclist at a separation distance of 4 feet (1.21 m). It can be seen that force-time history has a pressure phase and a suction phase similar to the results that have been measured in the field and with what has been reported in the cited work. The peak-to-peak (between the pressure and suction phases) force was calculated from the data presented in Figure 3.24.
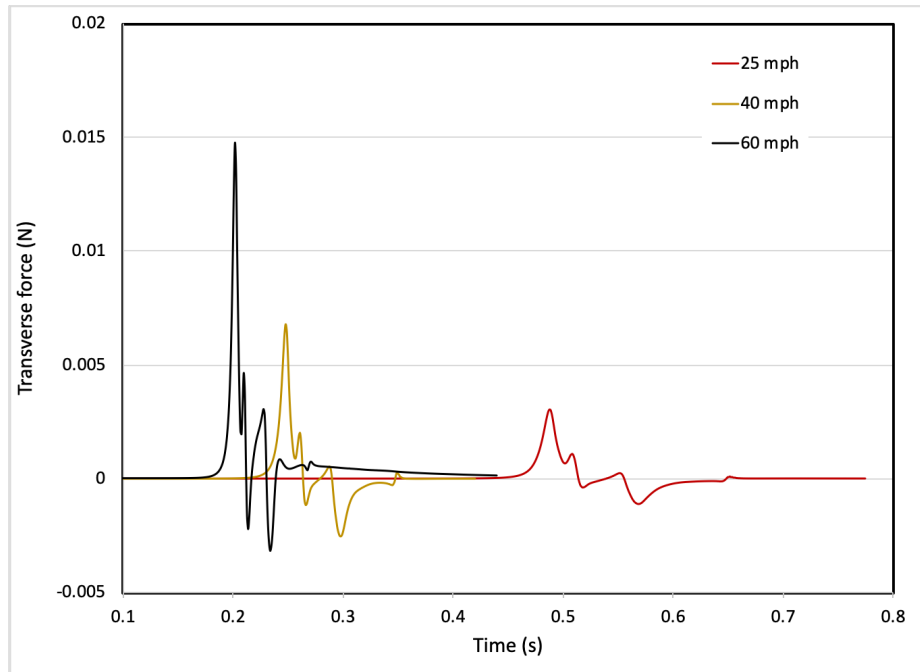
Figure 3.24 Transverse force time history on the cyclist at a separation distance of 6 feet (1.83 m).

The maximum force was 0.024 lb. (0.018 N) for the 60-mph case and the lowest was 0.0009 lb. (0.004 N) for the 25 mph run. The results trend was logical as the measured force decreased with decreasing the truck speed.

Figure 3.25 shows a comparison of the transverse forces induced on cyclists from the designed nine cases. It can be seen that the overall forces decreased with decreasing the vehicle speed and increasing the separation distances. The largest force was attributed to the case of 60 mph (26.82 m/s) and 2 ft. (0.61 m) separation distance. The results of the CFD have been compared to the wind tunnel as shown in Figure 3.26. It can be seen that both results have the same trend when changing the separation distance or the vehicle speed. Overall, the forces obtained from the CFD were higher than the wind tunnel values for all cases except the case of 25 mph (11.17 m/s) at 2 ft. (0.61m) separation distance. The highest and lowest percent of differences were 0.073% and 1.55%.

The trend from the CFD analysis and the wind tunnel test was similar to the trend of force values obtained from the field test. The forces increased with increasing vehicle speed and decreases with separation distance. There is no well-defined correlation that could be defined or established due to the scaling factor used in the CFD and in the wind tunnel.
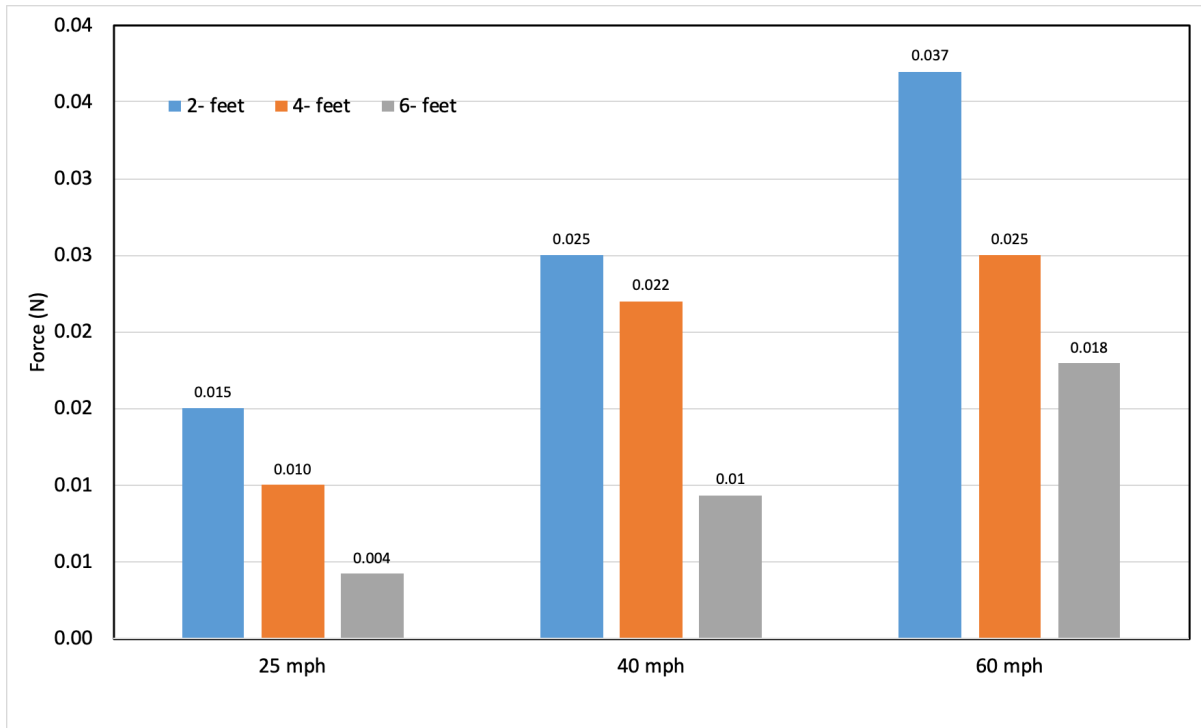
Figure 3.25 Transverse force on cyclist
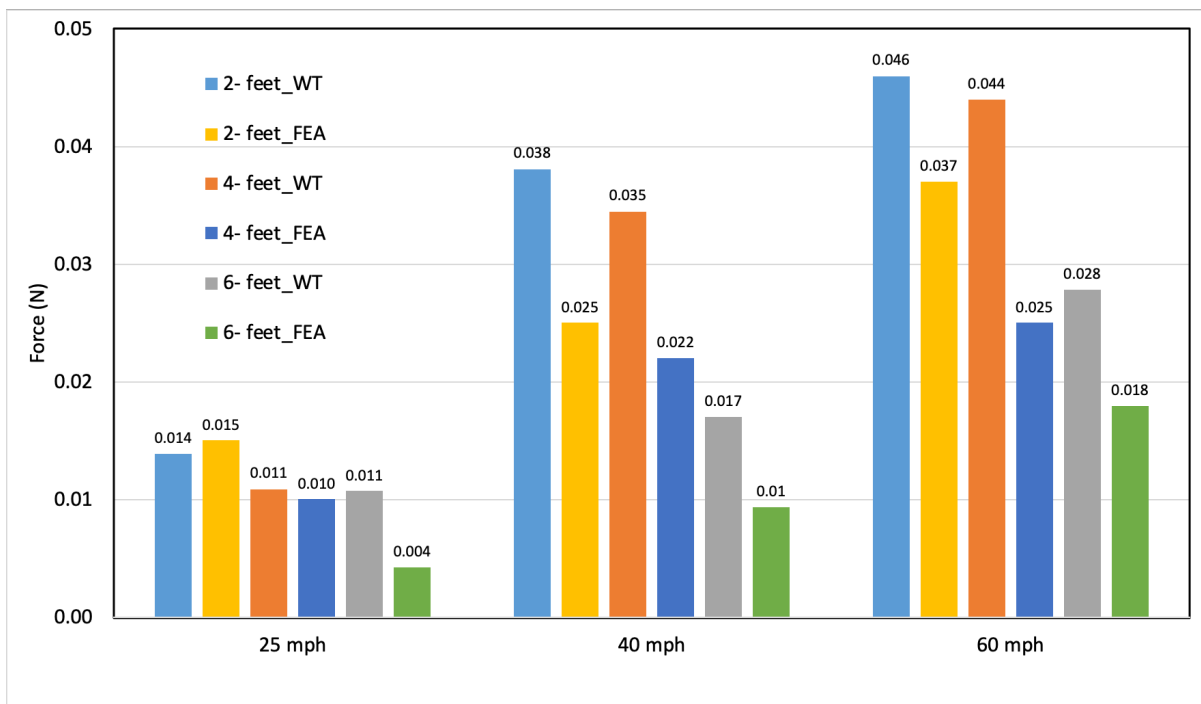for various vehicle speeds and separation distances (CFD).

Figure 3.26 Comparison between the CFD and wind tunnel results

In addition, a t-test has been done between the CFD and the wind tunnel results. It was found that the p-value had a value of 0.188> 0.05, which means that there were no significant differences between the two sets of results.

Overall, the results of the CFD and the wind tunnel are feasible and have the same trend. The CFD could be used to predict the forces on cyclists due to various vehicles and separation distances.

3.5 Conclusions

The present study presented an overview of real field experiments to investigate transverse force characteristics induced on cyclists by passing four types of vehicles under controlled and uncontrolled boundary conditions. The results of this study will be very beneficial for any potential future research on cyclist safety. The data generated from this study constitutes only a small portion of cyclist reactions that might involve more factors other than induced forces and moments. Those factors might be cyclist physical physiognomies, riding skill, road type, existence of bike lane or not, shoulder width, wind condition, riding features such as pedal position, bike stability, grade slope, and biker awareness of traffic, to name a few.

Cyclists experience lateral pressure and suction phase at a certain time frame when vehicles pass by them, which could be defined as the flip over phase which induces flipping over moments. In the present study, transverse forces and flipping moments on various types of cyclists induced by four types of overtaking vehicles were investigated. All the forces and moments were quantified by measuring wind speed using ultrasonic wind sensor positioned at various separation distances and under various vehicle speeds. Vehicle speeds were 25 mph, 40 mph, and 60 mph under separation distances of 2, 4 and 6 ft. The field tests were performed under controlled boundary conditions of using road section with very low traffic interference. In addition, uncontrolled tests on actual highway were performed. A correlation between the controlled and uncontrolled tests were established. All the studied parameters were assumed that the cyclists were stationary and vehicles were moving, so in the case of both the cyclist and the vehicle moving, the relative speed should be used. The established functional equations strictly apply only for vehicles and the cyclist types investigated in this study.

Overall, it was found that the flip over force (peak pressure to peak suction) increased with increasing potential side area of the cyclist, with increasing vehicle speed and decreasing separation distance. Multi-Regression analysis was performed and prediction equations of longitudinal and transverse

wind speeds were developed based on separation distance, vehicle speed, and vehicle type. Those equations could be used to predict force levels and characteristics on cyclists to assess cyclist safety. In addition, functions were developed to predict flipping moment for the various scenarios studied. The established functions can only be applied to the four types of the vehicles investigated in this study and under the investigated parameters. The reduction in truck speed and providing more shoulder width (separation distance) would be practical solutions to give a cyclist space to maneuver before moving into traffic.

The transverse forces induced on cyclists may represent a hazard to cyclists due to the sudden pressure and suction that push the cyclist away and then towards the vehicle. The rate of change of the transverse forces, combined with their magnitude, may cause a problem especially that those forces might cause lateral flipping tilt or moment. The cyclist might control this sudden force by applying self-adjusting force where the cyclist could change the bike direction. This immediate adjustment might take some time compared to the very short duration of the applied force.

The results of the FEM and the wind tunnel are very close, and it is feasible to perform CFD and FEA simulations for such a problem. However, the cost of computation is still a challenge.

Chapter 4: Conclusions and Recommendations

This study introduces two research studies that are intended to help enhancing transportation safety. The findings from this work will be compiled as a compendium for my dissertation. Each study is currently at a different point of completion. This chapter describes the objectives, current status, and remaining tasks for each study. The findings from this work will help provide countermeasures and solutions to improve transportation safety.

The World Health Organization (WHO) reports [1] that 1.35 million people die each year because of road traffic crashes and that vehicle collisions are the second leading cause of unintentional death worldwide (following poisoning as the first leading cause of unintentional death). The 2030 WHO goal is to decrease the number of crashes by 50%. The cost of traffic crashes is reported to be 3% of the total countries' income. In the USA, 33,650 deaths were reported in 2018 with 11.2 deaths per 100,000 population. In the state of Idaho, 73% of the 201 fatal vehicle crashes occurred in Idaho rural areas as reported by Insurance Institute for Highway Safety (IIHS) [2]. The National Highway Traffic Safety Administration (NHTSA) [3] reported that the economical and societal cost of traffic crashes is $871 B in a single year. Therefore, transportation safety and saving lives of people is a major topic that need to be studied and enhanced further.

A vendor-independent reliability testing approach for vehicle-to-infrastructure (V2I) communications in connected vehicle traffic signal system applications has been investigated. It provides an alternative to using the communication data reported by proprietary vendor-supplied interfaces. This study was based on building a rigorously tested translation model that uses measured Received Signal Strength Indicator (RSSI) from any V2I communication equipment to predict the corresponding Packet Delivery Ratio (PDR). This was achieved by correlating the signal strength, measured using a generic power meter, to PDR values reported in the communication interface of the equipment of different vendors. Both stationary and in-motion (10 to 40 mph) field data collection tests were conducted at three traffic intersections. These tests were performed over distances of up to 500 meters between the Roadside Units (RSUs) and the On-Board Units (OBUs). The results were statistically analyzed and logistic and linear regression models that predict PDR values were developed. A case study to test and validate this new PDR prediction model was conducted at two intersections in Boise, Idaho. Our prediction model will enable transportation system operators to test and validate the

efficiency of connected vehicle RSU/OBU communications at signalized intersection approaches under different traffic conditions, independent of vendor-provided tools.

The second topic of this research is related to the understanding of the unsteady wind flow exerted on cyclist by passing vehicles. There are many cases of cyclists being hit by the wind generated from passing trucks, however this unreliable evidence has not been investigated before in the USA. In 2019, there was 846 bicyclists killed in crashes with motor vehicles in the USA with an increase of 32% of pedestrian and cyclist fatalities between 2008 and 2019. The aerodynamic loads generated from moving vehicles trigger a concern on the stability and safety of cyclists which might lead to loss of control and consequently cyclist injury. The results of this study will significantly help identifying various factors affect safety of cyclists while in rural and urban areas. The key parameters investigated were the relative speed between cyclist and truck (25, 40, and 60 mph), vehicle type (semitrailer, Single unit truck, SUV, and pick-up truck), separation distance spacing between cyclist and the truck (2 ft., 4 ft, and 6 ft.), and various cyclist types. The wind transverse and longitudinal wind speeds have been used to drive equivalent transverse and longitudinal forces using the aerodynamic principles and therefore the flipping moment experienced by a cyclist. The data were generated through intensive field tests through controlled and uncontrolled environment. In addition, computational fluid dynamics models were built to investigate the feasibility of using computer simulations in predicting forces on cyclists. Finally, a 3D printed scaled truck and cyclist was tested in a wind tunnel under the same environments that were used in the computer simulations. The study concluded that wind speed prediction equations are a function of vehicle speed, separation distances, and vehicle type. The equations were derived based on the data collected from the field and were validated using the uncontrolled data set. In addition, flipping moment charts were developed for each type of the vehicles to offer a strong evidence of quantified flipping moments experienced by cyclists under various conditions. The computer simulations concluded that it is feasible to use computational fluid dynamics to model the whole environment of various wind speeds and separation distances for typical cyclists. Strong correlation between the computer simulations and the wind tunnel tests were obtained. The overall results from the field tests and the computer simulations and the wind tunnel are showing the same trend in terms of transverse and longitudinal wind forces experienced by cyclist.

4.1 Conclusions

The following conclusions have been drawn from the results of this study:

- Developed a vendor-independent reliability model for testing the communication reliability of V2I communications.

- An independent measurement of the RSSI using an RF power meter and a logistic expression was derived to relate the PDR to the vendor reported RSSI.

- A linear regression model was developed to fit the data between the vendor tool and the independent power meter. The best derived model gave an R^2 of 89% and an RMSE equal to 2.21%. The result was an expression for the PDR as a function of the measured RSSI. The developed statistical models have been used in a case study in two actual intersections in Boise, Idaho to evaluate the efficiency of two vendors' RSU.

- One important conclusion of this work is the repeatability to other vendors' equipment, environments, and types of intersections. As described, there are two aspects to these results, linking the PDR to RSSI and correlating measured RSSI with vendor reported RSSI. It is expected that the PDR would perform similar to the reported results versus RSSI because the underlying physical layer communication is implemented according to the DSRC standard; the discrepancies are in the higher layers of the network e.g. data link, network and application layers. However, the RSSI may vary among different vendors and may vary slightly with different power meters. Therefore, for any agency to reproduce our results, they may have to correlate the RSSI reported by both, their meters and RSU's or they may even need to develop a generalized model by collecting results from multiple meters and RSUs.

- The value our work is in the fact that it demonstrates how agencies only need to correlate the RSSI of their independent meters to vendor tools which does not require live field testing, only a testing setup that will ensure signals are received from low ranges of power to high power. Once this correlation is done, the PDR can be estimated as a function of RSSI. Overall, the results of this study provide a valuable independent technique for transportation agencies and USDOT to evaluate the efficiency of any RSU vendors' performance without accessing the specific vendors' software.

Cyclists experience lateral pressure and suction phase at a certain time frame when vehicles pass by them, which could be defined as the flip over phase which induces flipping over moments. In the present study, transverse forces and flipping moments on various types of cyclists induced by an overtaking four types of vehicles have been investigated. All the forces and moments were quantified by measuring wind speed using ultrasonic wind sensor positioned at various separation distances and under various vehicle speeds. Vehicle speeds were 25, mph, 40 mph, and 60 mph under separation distances of 2, 4 and 6 ft. The field tests were performed under controlled boundary conditions of using road section with very low traffic interference. In addition, an uncontrolled test on an actual

highway was performed. A correlation between the controlled and uncontrolled tests was established. All the studied parameters were assumed that the cyclists was stationary and vehicles were moving, so in the case of both the cyclist and the vehicle moving, the relative speed should be used. The specific conclusions of this study were the following:

- The established functional equations strictly apply only for vehicles and the cyclist types investigated in this study.

- Overall, it was found that the flip over force (peak pressure to peak suction) increased with increasing potential side area of the cyclist, with increasing vehicle speed and decreasing separation distance.

- Multi-Regression analysis was performed and prediction equations of longitudinal and transverse wind speeds were developed based on separation distance, vehicle speed, and vehicle type. Those equations could be used to predict force levels and characteristics on cyclists to assess cyclist safety.

- In addition, functions were developed to predict flipping moment for the various scenarios studied. The established functions can only be applied to the four types of the vehicles investigated in this study and under the investigated parameters. The reduction in truck speed and providing more shoulder width (separation distance) would be practical solution to give cyclist space to maneuver before moving into traffic.

- The transverse forces induced on cyclists may represent a hazard to cyclists due to the sudden pressure and suction that push the cyclist away and then towards the vehicle.

- The rate of change (force divided by time) of the transverse forces could cause a stability issue especially that those forces might cause lateral flipping moment. The cyclist might control this sudden force by applying self-adjusting force where the cyclist could change the bike direction. This immediate adjustment might take some time compared to the very short duration of the applied force.

- The results of the FEM and the wind tunnel are very close, and it is feasible to perform CFD and FEA simulations for such a problem. However, the cost of computation still a challenge.

References

References for Chapter 1

1. World Health Organization (WHO), https://www.who.int/news-room/fact-sheets/detail/road-traffic-injuries.

2. Insurance Institute for Highway Safety (IIHS) Highway Loss Data Institute. (2020). 4121 Wilson Boulevard, 6th floor Arlington, VA 22203. Status Report.

3. Blincoe, L. J., Miller, T. R., Zaloshnja, E., & Lawrence, B. A. (2015). *The economic and societal impact of motor vehicle crashes, 2010. (Revised)* (Report No. DOT HS 812 013). Washington, DC: National Highway Traffic Safety Administration.

References for Chapter 2

1. FHWA Vehicle to Infrastructure Deployment Guidance and Products, (2015). FHW A-HOP-15-015, Federal Highway Administration, Washington, DC, Washington, D.C.

2. Safety Pilot Model Deployment. Lessons Learned and Recommendations for Future Connected Vehicle Activities. (2015). FHWA-JPO-16-363, John A. Volpe National Transportation Systems Center, U.S. Department of Transportation, Washington, D.C..

3. Chowdhury, M., Rahman, M., Rayamajhi, A., Khan, S. M., Islam, M., Khan, Z., & Martin, J. (2018). Lessons Learned from the Real-World Deployment of a Connected Vehicle Testbed. Transportation Research Record, 2672(22), 10–23. https://doi.org/10.1177/0361198118799034.

4. FHWA Connected Vehicle Pilot Deployment (CV Pilots) Program. NYC CV Pilot Deployment Presentation (source: http://www.its.dot.gov/pilots/pdf/02_CVPilots_NYC.pdf).

5. Connected Vehicle Pilot Deployment Program Phase 2. Comprehensive Maintenance and Operations Plan. (2018). New York City, FHWA-JPO-17-457, New York City Department of Transportation (NYCDOT), Long Island City, NY.

6. Wyoming (WY) DOT Connected Vehicle Pilot Program. https://wydotcvp.wyoroad.info.

7. Connected Vehicle Pilot Deployment – Downtown Tampa. https://www.its.dot.gov/pilots/pdf/CVP_THEASystemDes ignWebinar.pdf

8. McGurrin (Noblis) Kevin Gay (ITS JPO). (2016). USDOT Guidance Summary for Connected Vehicle Pilot Site Deployments: Security Operational Concept. FHWA-JPO-16-338.

9. U.S. Government Accountability Office (GAO), Intelligent Transportation Systems: Vehicle-to-Infrastructure Technologies Expected to Offer Benefits but Deployment Challenges Exist. GAO-15-775. http://www.gao.gov/products/GAO-15-775. 2015.

10. G. S. Ching et al. (2007). Analysis of DSRC service over-reach inside an arched tunnel. *IEEE J. Sel. Areas Commun*. Volume: 25 (8): 1517–1525.

11. D. J. Jerry, L. Thomas, S. T. Panicker, R. Shalu, J. T. Mathew, and B. V. V. S. Joe. (2018). Safety Alert Systems Using Dedicated Short-Range Communication for on Road Vehicles. *International CET Conference on Control, Communication, and Computing*. 216–219.

12. W. Zheng, W. Jing, S. Chen, W. Nai, and D. Dong. (2013). Key Indices Analysis of IEEE 802.11p based Vehicle to Infrastructure System in Highway Environment. *Procedia - Soc. Behav. Sci*. Volume 96:188–195.

13. F. A. Teixeira, V. F. e Silva, J. L. Leoni, D. F. Macedo, and J. M. S. Nogueira. (2014). Vehicular networks using the IEEE 802.11p standard: An experimental analysis. *Veh. Commun*. Volume 1(2): 91–96.

14. B. Cheng, H. Lu, A. Rostami, M. Gruteser, and J. B. Kenney. (2018). Impact of 5.9 GHz spectrum sharing on DSRC performance. *IEEE Vehicular Networking Conference*.p215–222.

15. M. E. Renda, G. Resta, P. Santi, F. Martelli, and A. Franchini. (2016). IEEE 802.11p VANets: Experimental Evaluation of Packet Inter-Reception Time. *Comput. Commun*. p26–38.

16. K. Hong, D. Xing, V. Rai, and J. Kenney. (2009). Characterization of DSRC Performance as a Function of Transmit Power. *ACM VANET*.p. 63-68.

References for Chapter 3

1. Gaither TW, Sanford TA, Awad MA, et al. (2018). Estimated total costs from non-fatal and fatal bicycle crashes in the USA: 1997–2013. Injury Prevention. 24:135-141.

2. Cali, P. M., Covert, E. E. (2000). Experimental Measurements of the Loads Induced on an Overhead Highway Sign Structure by Vehicle-Induced Gusts. J. Wind Eng. & Ind. Aero. 84, 87-100.

3. Quinn, A. D., Baker, C. J., Wright, N. G. (2001). Wind and Vehicle Induced Forces on Flat Plates – Part 2: Vehicle Induced Force. J. Wind Eng. & Ind. Aero. 89, 831-847.

4. Sanz-Andrés, A., Laverón, A., Cuerva, A., Baker, C. (2004). Vehicle-Induced Force on Pedestrians. J. Wind Eng. & Ind. Aero. 92, 185-198.

5. Lichtneger, P., Ruck, B. (2015). Full scale experiments on vehicle induced transient loads on roadside plates. J. Wind Eng. & Ind. Aero. 136, 73-81.

6. Gromke, G., and Ruck, B. (2019). Aerodynamic loads on a cyclist while overtaking by a vehicle. Fachtagung "Experimentelle Strömungsmechanik, Erlangen.

7. Lubitz, W., D. and Rubie, R. Wind Loads on Cyclists Due To Passing Vehicles. (2018). Proceedings of The Canadian Society for Mechanical Engineering International Congress. CSME International Congress 2018 May 27-30, Toronto, On, Canada.

8. Walton, D., Dravitzki, V.K., Cleland, B.S., Thomas, J.A., Jackett, R. (2005). Balancing the needs of cyclists and motorists. Land Transport New Zealand Research Report No. 273. 92pp.

9. Llorca, C., Angel-Domenech, A., Agustin-Gomez, F., Garcia, A. (2017) Motor vehicles overtaking cyclists on two-lane rural roads: analysis on speed and lateral clearance. Safety science. 92, 302-310.

10. FHWA, (1977). A Bikeway Criteria Digest - the ABCD's of Bikeways. Federal Highway Administration, US Department of Transport.

11. Lee, H.S.-H., (2009). The Aerodynamic Effects of Passing Trains to Surrounding Objects and People. Federal Railroad Administration, United States.

12. Federal Size Regulations for Commercial Motor Vehicles. (2004). U.S. Department of Transportation
Federal Highway Administration.

13. Gritskevich, M., Garbaruk, A., Schütze, J., Menter, F. (2011) Development of DDES and IDDES Formulations for the k-ω Shear Stress Transport Model. Flow Turbulence Combust DOI 10.1007/s10494-011-9378-4.

14. Hammad, A., and Xing, T. (2017). Aerodynamic Effects on Two-Lane Rural Highway Safety. The Pacific Northwest Transportation Consortium (PacTrans), Region 10 University Transportation Center (UTC), U.S. Department of Transportation (USDOT).

15. ANSYS Fluent Theory Guide, Release 17.1, April 2017.

16. Spalart, P.R., Deck, S., Shur, M.L., Squires, K.D., Strelets, M.K. and Travin, A., (2006). A new version of detached-eddy simulation, resistant to ambiguous grid densities. Theoretical and computational fluid dynamics, 20(3), pp.181-195.

17. Munson, Young and Okiishi. (2004). Fundamental of Fluid Mechanics. Wiley &Son.

Appendix A: Wind sensor 86000 specs (http://www.youngusa.com/products/1/)

Wind Speed: 0-75 m/s
Resolution: 0.01 m/s
Starting Threshold: 0.01 m/s
Accuracy: 30 m/s ± 2% or 0.1 m/s, 75 m/s ± 3% Response Time: < 0.25 seconds
Wind Direction: 0 to 360 degrees Resolution: 0.1 degree
Starting Threshold: 0.01 m/s Accuracy: ± 2 degrees
Response Time: < 0.25 seconds
Serial Output: RS232 or RS485
Formats: ASCII, ASCII polled, NMEA, RMYT
SDI-12
Baud: 1200, 4800, 9600, 19200, 38400
Wind Units: m/s, knots, mph, kmph
Wind Format: Speed & Direction or U & V Status Indicator: Standard with ASCII & NMEA
Analog Outputs: 0-5000 mV or 4-20 mA
Analog Wind Scale: 0-100 m/s
Analog Direction Scale: 0-360 or 0-540 degrees
Output Update Rate: 0.1 to 20 Hz
Power Requirement:
Sensor: 10-30 VDC < 20 mA typical Heater: 24 VDC, 2.5 A (Model 86004 Only)
Environmental:
Operating Temperature: -40 to +60°C Protection Class: IP65
Dimensions: 29 cm high x 11 cm wide Weight: 0.4 kg (0.9 lb)
Shipping Weight: 1.6 kg (3.5 lb)